NIST Technical Note 1994

Calibration of Dynamic Pressure in a Tubing System and Optimized Design of Tube Configuration: A Numerical and Experimental Study

Matthew Kovarek
Luke Amatucci
Keith A. Gillis
Florian A. Potra
James Ratino
Marc Levitan
DongHun Yeo

This publication is available free of charge from:
https://doi.org/10.6028/NIST.TN.1994

National Institute of Standards and Technology
U.S. Department of Commerce

NIST Technical Note 1994

Calibration of Dynamic Pressure in a Tubing System and Optimized Design of Tube Configuration: A Numerical and Experimental Study

Matthew Kovarek
Department of Chemical Engineering
University of Maryland, Baltimore County, Baltimore, MD 21250

Luke Amatucci
Department of Aerospace Engineering
University of Maryland, College Park, MD 20742

Keith A. Gillis
Physical Measurement Laboratory
National Institute of Standards and Technology, Gaithersburg, MD 20899-8360

Florian A. Potra
Information Technology Laboratory
National Institute of Standards and Technology, Gaithersburg, MD 20899-8910

James Ratino
Marc Levitan
DongHun Yeo
Engineering Laboratory
National Institute of Standards and Technology, Gaithersburg, MD 20899-8611

This publication is available free of charge from:
https://doi.org/10.6028/NIST.TN.1994

June 2018

U.S. Department of Commerce
Wilbur L. Ross, Jr., Secretary

National Institute of Standards and Technology
Walter Copan, NIST Director and Undersecretary of Commerce for Standards and Technology

Certain commercial entities, equipment, or materials may be identified in this document in order to describe an experimental procedure or concept adequately. Such identification is not intended to imply recommendation or endorsement by the National Institute of Standards and Technology, nor is it intended to imply that the entities, materials, or equipment are necessarily the best available for the purpose.

National Institute of Standards and Technology Technical Note 1994
Natl. Inst. Stand. Technol. Tech. Note 1994, 67 pages (June 2018)
CODEN: NTNOEF

This publication is available free of charge from:
https://doi.org/10.6028/NIST.TN.1994

DISCLAIMER

(1) The policy of the NIST is to use the International System of Units in its technical communications. In this document however, works of authors outside NIST are cited which describe measurements in certain non-SI units. Thus, it is more practical to include the non-SI unit measurements from these references.

(2) Certain trade names or company products or procedures may be mentioned in the text to specify adequately the experimental procedure or equipment used. In no case does such identification imply recommendation or endorsement by the National Institute of Standards and Technology, nor does it imply that the products or procedures are the best available for the purpose.

This publication is available free of charge from: https://doi.org/10.6028/NIST.TN.1994

This publication is available free of charge from: https://doi.org/10.6028/NIST.TN.1994

ABSTRACT

Accurate prediction of aerodynamic pressures on buildings is a key factor in the estimation of wind loads. Analytical and numerical approaches to the estimation of pressures on buildings have limited capabilities. The experimental approach faces a challenge: pressures on building models cannot be directly measured by pressure sensors. Rather, a tubing system connecting the model to the sensor is required. Owing to acoustic and visco-thermal effects associated with the fluid action on the system's thin, circular tubes, the pressure waves propagating inside the tubes cause the pressure fluctuations being measured to experience amplitude changes and phases shift that depend upon the fluctuations' frequencies. It is therefore necessary to develop a correction procedure for converting the distorted pressure data measured by transducers into pressures that differ insignificantly from the actual aerodynamic pressures on the model.

To address this issue, a review was performed of topics related to the aspects of Navier-Stokes equations, thermodynamic effects, wave propagation, and mass and energy conservation as applied to sinusoidal air motions in cylindrical tubing systems, and a MATLAB-based program, called *CalibPress* (version 1.0), was developed to calibrate the amplitude change and phase lag in tubing configurations used in wind tunnel testing. To validate the requisite amplitude ratio and phase lag transfer functions, we employed an experimental method using a function generator, a speaker system, and a theoretical method based on the lumped-element transmission line model.

The parameters accounted for in *CalibPress* include not only tube dimensions of tube length and inner diameters, but also air properties including temperature, atmospheric pressure, and relative humidity. The program uses the visco-thermal parameters of air accurately calculated from the REFPROP program. The results showed that the atmospheric pressure and temperature can influence significantly the pressures measured in a tubing system.

An optimization design procedure of the tubing system consisting of two tubes and one restrictor was developed for minimization of tubing effects on pressure measurements.

Keywords: Calibration; optimization; pressure measurements; transfer functions; tubing system; wind tunnel experiment.

This publication is available free of charge from: https://doi.org/10.6028/NIST.TN.1994

ACKNOWLEDGEMENTS

With mentoring advice from Dr. DongHun Yeo, Mr. Matthew Kovarek developed a program for calibration of dynamic pressures via a tubing system, Mr. Luke Amatucci carried out experiments for validation of the numerical results, and Mr. Chongqing Fan did preliminary experimental work. Dr. Marc Levitan provided helpful discussions and insightful advice on the experimental device designed by Mr. James Ratino. Dr. Keith Gillis provided insightful comments and validated the numerical results using his lumped-element transmission line model. Dr. Florian Potra advised the optimization procedure in tubing systems. The authors are indebted to Dr. Eric Lemmon and Dr. Harrison Skye for enabling them the use of the program REFPROP and a function generator, respectively, to Dr. John D. Homes and Dr. Emil Simiu for their careful reviews, and to Mr. Addison Pemberton and Mr. Ryan Pemberton of Scanivalve, who graciously answered questions on the use of their equipment.

This publication is available free of charge from: https://doi.org/10.6028/NIST.TN.1994

CONTENTS

This publication is available free of charge from: https://doi.org/10.6028/NIST.TN.1994

LIST OF FIGURES

This publication is available free of charge from: https://doi.org/10.6028/NIST.TN.1994

This publication is available free of charge from: https://doi.org/10.6028/NIST.TN.1994

LIST OF TABLES

This publication is available free of charge from: https://doi.org/10.6028/NIST.TN.1994

This publication is available free of charge from: https://doi.org/10.6028/NIST.TN.1994

1. INTRODUCTION

Accurate prediction of aerodynamic pressures on buildings is a key factor in the estimation of wind loads. Analytical and numerical approaches to the estimation of pressures on buildings have limited capabilities. The experimental approach faces a challenge: pressures on building models cannot be directly measured by pressure sensors. Rather, a tubing system connecting the model to the sensor is required. Owing to acoustic and visco-thermal effects associated with the fluid action on the system's thin, circular tubes, the pressure waves propagating inside the tubes cause the pressure fluctuations being measured to experience amplitude changes and phases shift that depend upon the fluctuations' frequencies. It is therefore necessary to develop a correction procedure for converting the distorted pressure data measured by transducers into pressures that differ insignificantly from the actual aerodynamic pressures on the model.

To address this issue, a review was performed of topics related to the aspects of Navier-Stokes equations, thermodynamic effects, wave propagation, and mass and energy conservation as applied to sinusoidal air motions in cylindrical tubing systems, and a MATLAB-based program, called *CalibPress* (version 1.0) was developed to calibrate the amplitude change and phase lag in tubing configurations used in wind tunnel testing. To validate the requisite amplitude ratio and phase lag transfer functions, an experimental device was designed and built using a function generator and a speaker. In addition, the validation accounted for phase changes due to the measuring sequence in a multi-channel pressure scanner.

The report contains the following chapters: Introduction, Characteristics of pressures measured by using tubing systems, Program development, Experimental measurements and comparisons, Parameters affecting measured pressures, Optimization of tubing systems, and Conclusions.

This publication is available free of charge from: https://doi.org/10.6028/NIST.TN.1994

2. CHARACTERISTICS OF PRESSURES MEASURED BY TUBING SYSTEMS

2.1 Tubing System

Due to the shape and placement of models used in wind tunnel experiments, pressure sensors cannot typically be directly connected to pressure taps placed on the models. A tubing system is required to transmit the pressure waves from the pressure taps to the sensors. The pressures measured by the sensors through a tubing system are not equal to the pressures at the taps located on the surface of the model. To develop the requisite correction it is necessary to model the behavior of the fluid inside the confined tubing system.

A simple three-dimensional tubing system consisting of three tubes and two volumes is shown in Figure 2.1.

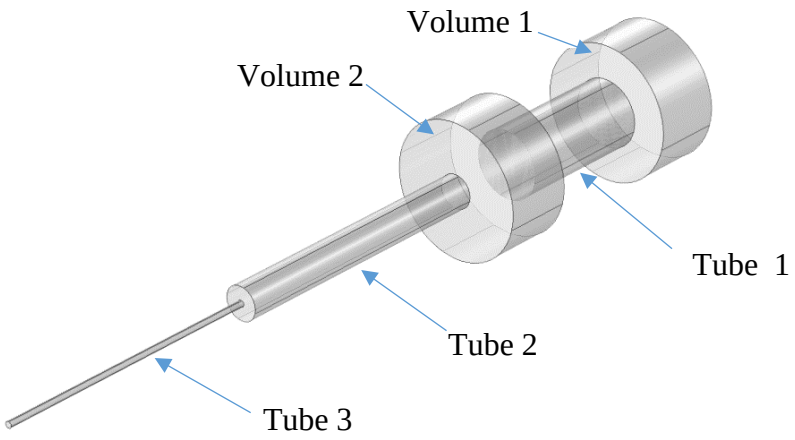

Figure 2.1. Three-dimensional representation of a system with three tubes and two volumes.

2.2 Effects of Tubing System on Pressure Measurement

2.2.1 Amplitude distortion

The amplitudes of pressure waves that propagate within a tubing system experience frequency-dependent distortions affected by the lengths and diameters of the tubes, and by air properties such as the atmospheric pressure, air temperature, speed of sound, specific heat at constant pressures and at constant temperature, and relative humidity. The description of the air motion in tubing systems can be obtained from the Navier-Stokes equations, the equation of continuity, the equation of state, and the energy conservation equation.

This publication is available free of charge from: https://doi.org/10.6028/NIST.TN.1994

Figure 2.2 illustrates a hypothetical tubing system with N tubes and N volumes. Pressure p_N represents the original pressure of interest and p_1 is the pressure propagated through circular Tube N-1 to Tube 1 with intermediate hypothetical transducers with Volume N-1 to Volume 1.

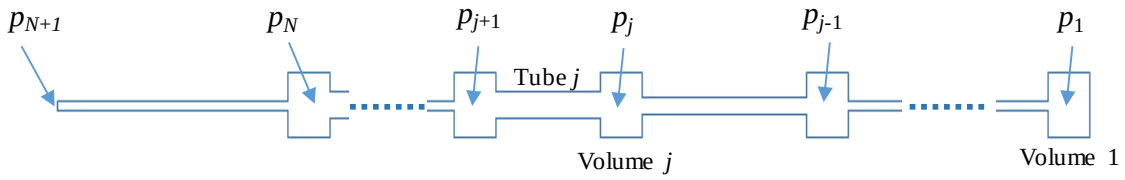

Figure 2.2 Representation a tube system of N tubes and N volumes.

For the tubing system shown in Figure 2.2, a recursion formula for the ratio of pressure at j to pressure at j-1 (Bergh and Tijdeman 1965) can be described as:

for $j = 1$

$$\frac{p_1}{p_2} = \left\{ \cosh(\theta_1 L_1) + \frac{V_1}{V_{t,1}} \left(\sigma_j + \frac{1}{k_{p,1}} \right) n_1 \theta_1 L_1 \sinh(\theta_1 L_1) \right\}^{-1} \tag{2.1a}$$

for $j = 2, 3, \ldots, N$

$$\frac{p_j}{p_{j+1}} = \left\{ \cosh(\theta_j L_j) + \frac{V_j}{V_{t,j}} \left(\sigma_j + \frac{1}{k_{p,j}} \right) n_j \theta_j L_j \sinh(\theta_j L_j) + \frac{V_{t,j-1}}{V_{t,j}} \frac{\theta_{j-1}}{\theta_j} \frac{L_j}{L_{j-1}} \frac{J_o(\alpha_j)}{J_o(\alpha_{j-1})} \frac{J_2(\alpha_{j-1})}{J_2(\alpha_j)} \frac{\sinh(\theta_j L_j)}{\sinh(\theta_{j-1} L_{j-1})} \left[\cosh(\theta_{j-1} L_{j-1}) - \frac{p_{j-1}}{p_j} \right] \right\}^{-1} \tag{2.1b}$$

where

$D_{t,j}$ = the thermal diffusivity in the definition of β_j

J_η (x) = Bessel function of the first kind of order η

Pr = Prandtl number

$V_{t,j} = \pi r_{t,j}^2 L_j$, Volume of tube j with length L_j and diameter $r_{t,j}$

V_j = Volume of Transducer j

c = Speed of sound

$$n_j = \left[1 + \frac{\gamma - 1}{\gamma} \frac{J_2(\alpha_j \sqrt{\mathrm{Pr}})}{J_0(\alpha_j \sqrt{\mathrm{Pr}})}\right]^{-1}, \text{ Polytropic factor of Tube } j$$

$$k_{p,j} = \left| \frac{\gamma}{1 + 3(\gamma - 1)\left(\beta_j^{-2} r_{t,j}^{-2}\right)\left[\beta_j r_{t,j} \coth\left(\beta_j r_{t,j}\right) - 1\right]} \right|, \text{ Polytropic parameter of Tube } j$$

$\alpha_j = i^{3/2} r_{t,j} \sqrt{\frac{\rho\omega}{\mu}} =$ Shear wave number of Tube j

$\beta_j = (1+i) \Big/ \sqrt{2D_{t,j}/\omega}$ in the definition of $k_{p,j}$

γ = Ratio of specific heat

σ_j = Dimensionless increase in Transducer j due to diaphragm deflection

$$\theta_j = \frac{\omega}{c} \sqrt{\frac{\gamma}{n_j}} \sqrt{\frac{J_0(\alpha_j)}{J_2(\alpha_j)}}, \text{ Reduced frequency of Tube } j$$

ρ = Density of air

ω = Angular frequency of pressure wave.

One difference between Eqs. 2.1 and its counterpart in Bergh and Tijdeman (1965) used in this study is the value of the polytropic parameter (k_p). While the earlier study assumed it to be a constant equal to the specific heat ratio, in this study the polytropic parameter is assumed to be a function on which details are given in Appendix B, with lower and upper bounds equal to 1 and to the specific heat ratio (i.e., approximately 1.4), respectively. For details see Appendix B. Figure 2.3 shows an example of the polytropic parameter in a simple tubing system as a function of frequency. Our study shows that the difference between the pressure ratios obtained by assuming the validity of the two assumptions regarding both calculations of the polytropic parameter is less than a few percent. Note that the equation of the polytropic parameter used in Eqs. 2.1 is identical to Eq. B.16.

The amplitude ratio of the original pressure p_N to the distorted pressure p_1 measured by the pressure transducer via the tubing system can be calculated as

This publication is available free of charge from: https://doi.org/10.6028/NIST.TN.1994

$$\left|\frac{p_1}{p_{N+1}}\right| = \left|\frac{p_1}{p_2}\frac{p_2}{p_3}\cdots\frac{p_N}{p_{N+1}}\right|. \tag{2.1}$$

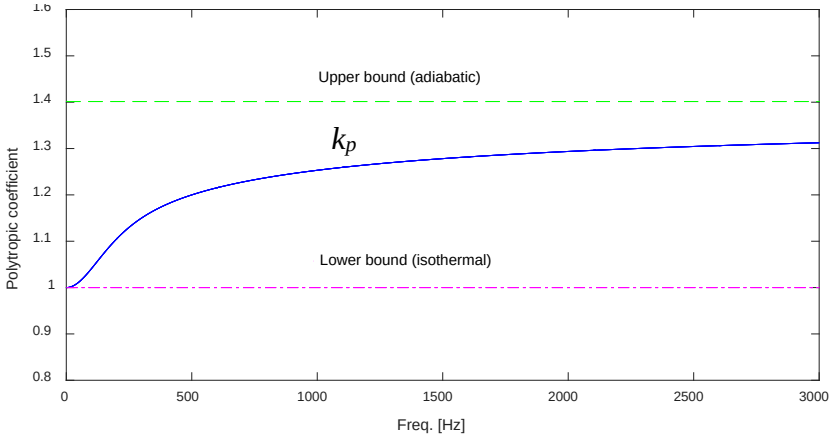

Figure 2.3 Polytropic parameter.

2.2.2 Phase lag

In addition to the amplitude, the phase angle of the pressures is also changed. The phase lag between p_1 and p_N, ϕ_{lag}, can be calculated as

$$\phi_{\text{lag}} = \phi_1 - \phi_{N+1} = \tan^{-1}\left[\frac{\text{Im}(p_1/p_{N+1})}{\text{Re}(p_1/p_{N+1})}\right] \tag{2.2}$$

where ϕ_N is the phase angle of the original pressure data p_N and ϕ_1 is the phase angle of the pressure data p_1 measured by the pressure transducer 1 (Figure 2.2). Re(x) and Im(x) are the real part and the imaginary part of x, respectively.

This publication is available free of charge from: https://doi.org/10.6028/NIST.TN.1994

This publication is available free of charge from: https://doi.org/10.6028/NIST.TN.1994

2.2.3 Helmholtz Resonance

The Helmholtz resonance phenomenon consists of the vibration of a volume of gas near the open hole of a container filled with that gas. The vibration is due to the spring-like behavior of the gas inside the container. The Helmholtz resonance frequency, f_H, in a tubing system consisting of a single tube and transducer is estimated by the following equation (Elson and Soedel 1972)

$$f_H = \frac{c}{2\pi L_t}\frac{1}{\sqrt{R}} \tag{2.3}$$

where

c = Speed of sound [m/s]

L_t = Length of tube sytem [m]

R = V_{tran}/V_{tube} (Ratio of transducer volume to tube volume).

The tubing system should be designed so that the Helmholtz frequency is much higher than the highest frequency of the pressures to be measured. The resonance frequency will increase when the tube diameter increases but its length decreases. This consideration should be taken into account when designing the tubing/transducer system or attempting to utilize the equations introduced in Sections 2.2.1 and 2.2.2.

The effects of the Helmholtz resonance on the transfer functions will be more noticeable for tubes with larger diameters and smaller volume of transducers. From a preliminary investigation on the tubing system used in this study, the Helmholtz resonant phenomenon is significantly reduced by inherent damping of tubes with small diameters (i.e., 0.86 mm and 1.36 mm).

This publication is available free of charge from: https://doi.org/10.6028/NIST.TN.1994

3. PROGRAM DEVELOPMENT

A MATLAB GUI (graphical user interface)-based program called *CalibPress* (version 1.0), was developed for calculations based on the recursion formulas of Eqs. 2.1 to 2.3 and the real time visualization of results. The program requires inputting the primary parameters (lengths and diameters of the tubes, ambient temperature, and atmospheric pressure). For accurate predictions in a wide range of experimental conditions, it is also necessary to obtain physical properties of air over a range of temperatures and pressures. The secondary parameters needed for the recursion formulas are density, viscosity, thermal conductivity, constant pressure heat capacity, constant volume heat capacity, and the speed of sound in air. The program has options for determining the secondary parameters by the REFPROP program (Lemmon and Huber 2015) or by user input. The relative humidity of real air can be also calculated by the REFPROP or the ASTM Wexler method (ASTM 2015) or determined by user input.

Once all parameters are provided, the program can generate transfer functions for the amplitude ratio and phase lag as functions of pressure fluctuating frequency, based on Eq. 2.2 and Eq. 2.3, respectively, for a tubing system of up to 10 tubes and 10 transducer volumes, by executing the “Plot” button shown at the bottom of the program GUI. The transfer functions can also be saved in the format which can be read by MATLAB or EXCEL software. A tubing system with one restrictor can be designed aiming at minimizing the difference between the highest and the lowest value of amplitude ratios.

This GUI-based program consists of six pages: 1) Program Information, 2) Tube Dimensions, 3) Physical Parameters, 4) Relative Humidity Calculator, 5) Optimization, and 6) Further Information. At each page a general information menu is created to outline the overall procedures of the program. The user can call this drop-down menu, which is located next to the save drop-down menu at the top of the program. The program starts by executing ‘dynamic_pressure.m.’

This publication is available free of charge from: https://doi.org/10.6028/NIST.TN.1994

3.1 Program Page One: Program Information

Once the MATLAB script 'dynamic_pressure.m' is executed, Page One appears on the screen as seen in Figure 3.1. This provides a general overview of the program including all the additional submenus. By changing items in the navigation menu, Page One can be shifted into another page mentioned in the following sections.

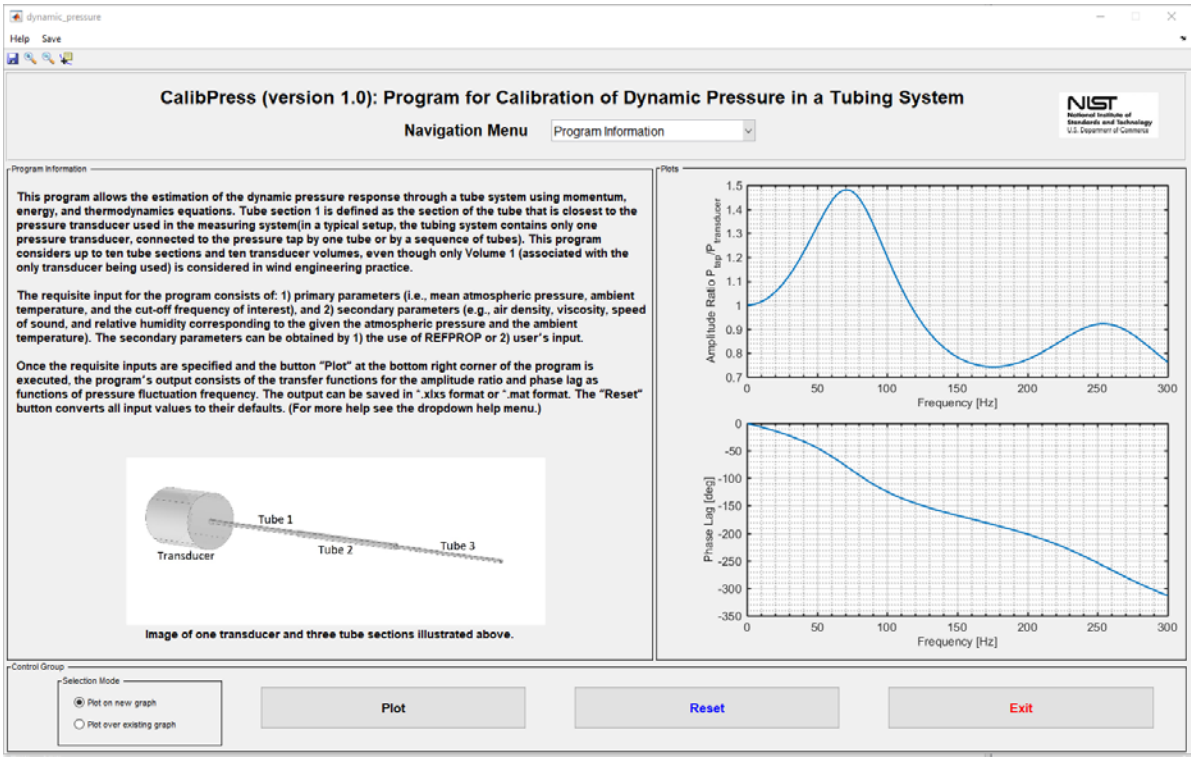

Figure 3.1 Screen-shot of GUI for a single tube/volume system.

This publication is available free of charge from: https://doi.org/10.6028/NIST.TN.1994

3.2 Program Page Two: Tube Dimensions

Page Two deals with the input information on tubes for up to a ten tube/volume tubing system. The input consists of: i) the lengths and diameters of tubes and ii) the volumes of the transducers, as shown in Figure 3.2. The tube connected to a pressure transducer is assigned to "Tube Section 1." The volume of the associated transducer is given to "Transducer Volume" in "Tube Section 1." If only one transducer is used at the end of Tube 1, the volumes of the transducers other than Tube 1 should be zero. The dimensions are in mm.

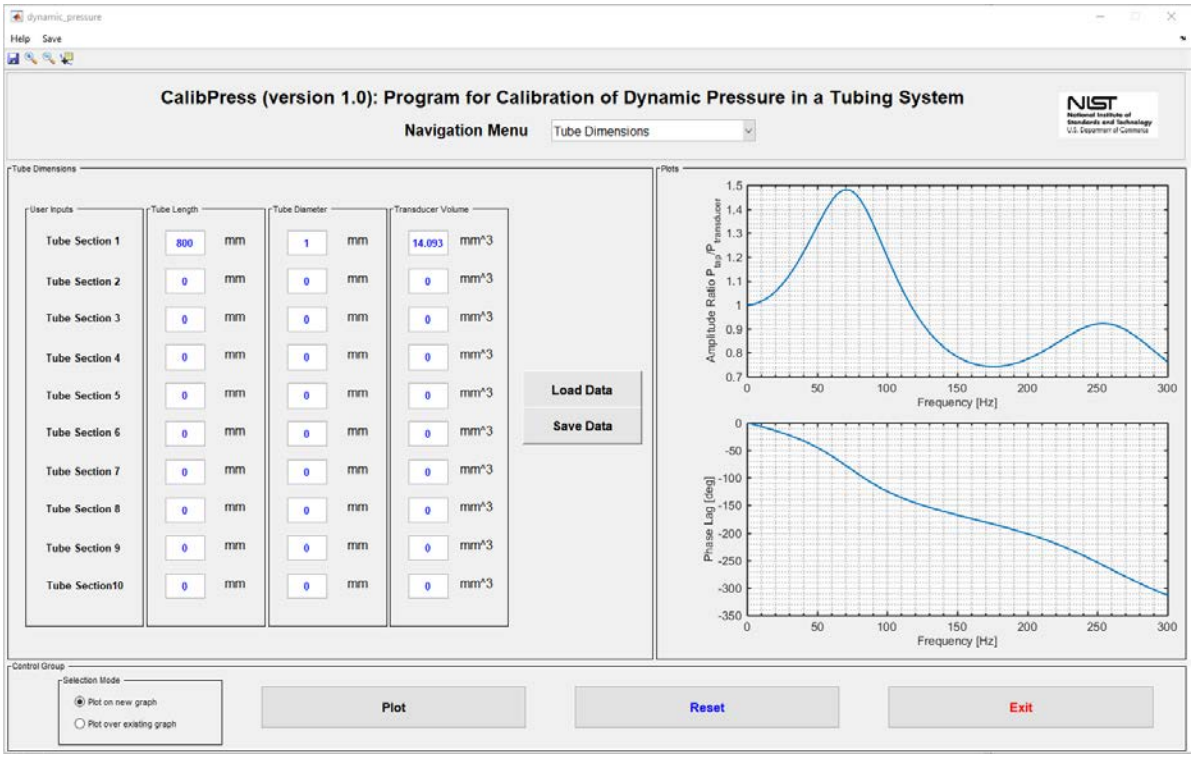

Figure 3.2 Screen-shot of GUI for input of number and dimensions of tube sections.

This publication is available free of charge from: https://doi.org/10.6028/NIST.TN.1994

3.3 Program Page Three: Physical Parameters

Page Three, as shown in Figure 3.3, contains inputs of i) primary parameters: mean atmospheric pressure, ambient temperature, maximum frequency of pressure fluctuations of interest and the transducer volume expansion factor (σ in Eqs. 2.1), and ii) secondary parameters: thermal diffusivity, density and viscosity of air, isobaric heat capacity (c_p), isochoric heat capacity (c_v), speed of sound, and thermal conductivity. These secondary parameters can be calculated from the given primary parameters by REFPROP (Lemmon and Huber 2015). Alternatively, when the secondary parameters described above are available from experiments or REFPROP is not available, they can be determined by the user input. In this case, inputs for mean atmospheric pressure and ambient temperature will be inactivated. The transducer volume expansion factor could be assumed to be zero unless it is accurately obtained from experiments. Once the primary and secondary parameters are determined, the program can calculate the heat capacity ratio, the polytropic parameter, and the Prandtl number, which are also needed to calculate transfer functions for the amplitude ratios and phase lags of the pressure fluctuations (see Eq. 2.1). The polytropic parameters of the tubes are visualized in a graph shown at the bottom left of the page.

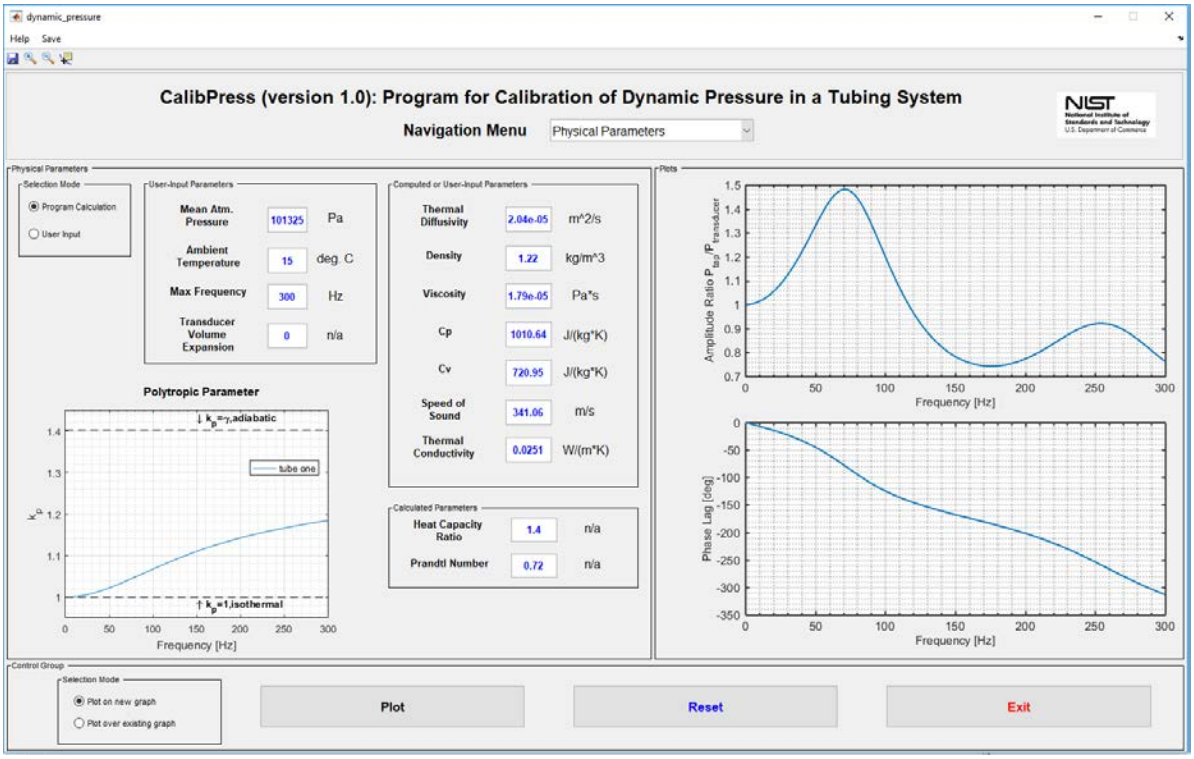

Figure 3.3 Screen-shot of GUI for input of physical parameters.

This publication is available free of charge from: https://doi.org/10.6028/NIST.TN.1994

3.4 Program Page Four: Relative Humidity Calculator

Page Four considers the relative humidity of air (Figure 3.4), which is calculated by REFPROP (Lemmon and Huber 2015) or the ASTM Wexler method (ASTM 2015) if users provide wet and dry bulb temperatures, or can be specified by the user input. Regardless of whether REFPROP is available, the ASTM Wexler method can calculate the relative humidity by the procedure summarized in Appendix A. Note that the button "Retrieve Data" can bring the input values of atmospheric pressure and ambient pressure from Page Two.

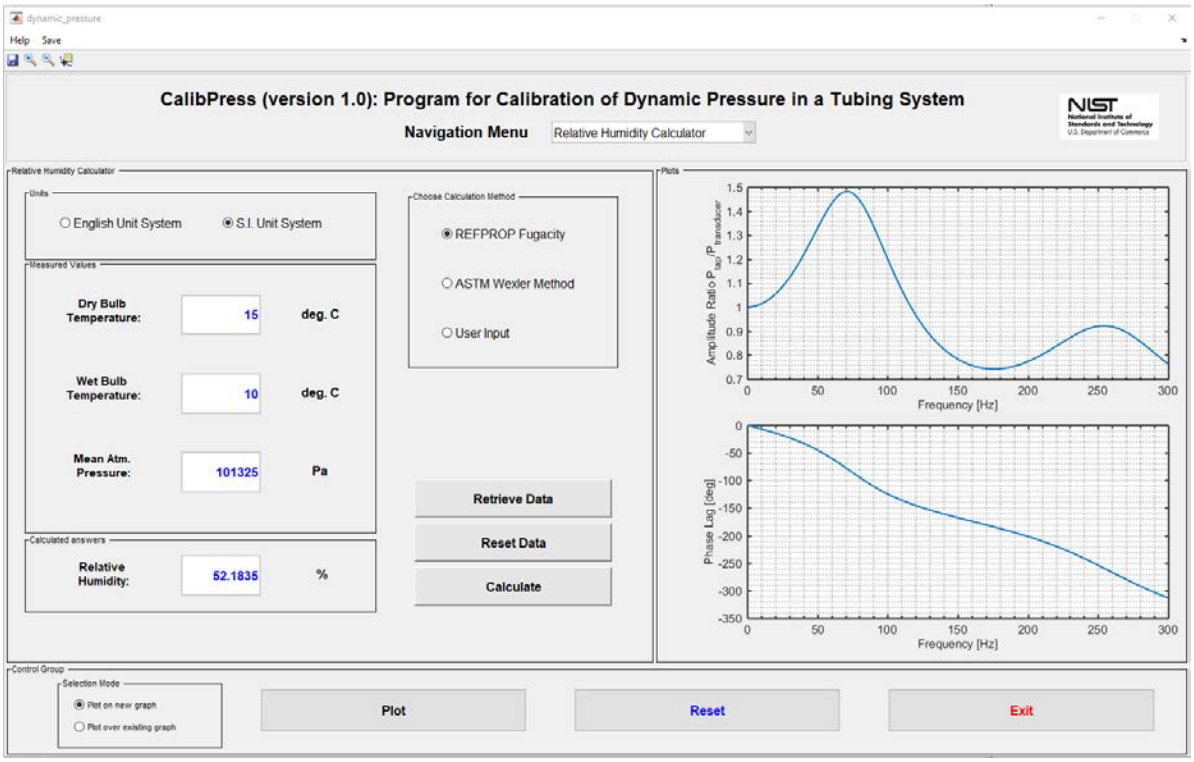

Figure 3.4 Screen-shot of relative humidity calculator.

This publication is available free of charge from: https://doi.org/10.6028/NIST.TN.1994

3.5 Program Page Five: Optimization

The program can achieve the design of a tubing system that consists of two tubes (Tubes 1 and 5 in Fig. 3.5), one restrictor that consists of Tubes 2 to 4, a pressure tap (Tube 6), and a pressure hole in the model wall (Tube 7). Tube 1 is a tube connecting a transducer (i.e., a pressure scanner) to one end of the restrictor, and Tube 5 is a tube connecting the pressure tap to the other end of the restrictor. Once a user specifies (1) the diameters of Tubes 1 and 5, (2) the diameters and the lengths of Tubes 2, 4, 6, and 7, (3) the lower and upper bounds of varying parameters (i.e., the lengths of Tubes 1 and 5 and their total length, and the diameter and length of Tube 3), the program calculates the optimized values of the varying parameters for minimizing the objective function (Eq. 6.1), written in red, by executing "Optimize" button (see Fig. 3.6). The details of the optimization procedure are summarized in Section 6.1. The selected tubing configuration can be transferred to Page Dimensions by clicking "Send to Tube Dimensions." Note that the all environmental information for the calculation of the transfer functions (shown in Pages "Physical Parameters" and "Relative Humidity Calculator") should be specified in advance for optimizing the tubing system.

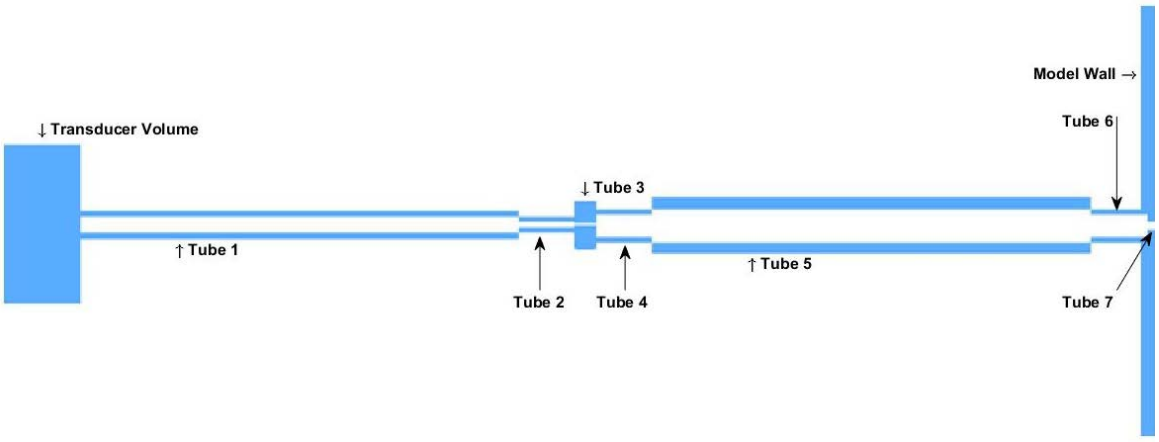

Figure 3.5 Configuration of a tubing system for optimization procedure.

This publication is available free of charge from: https://doi.org/10.6028/NIST.TN.1994

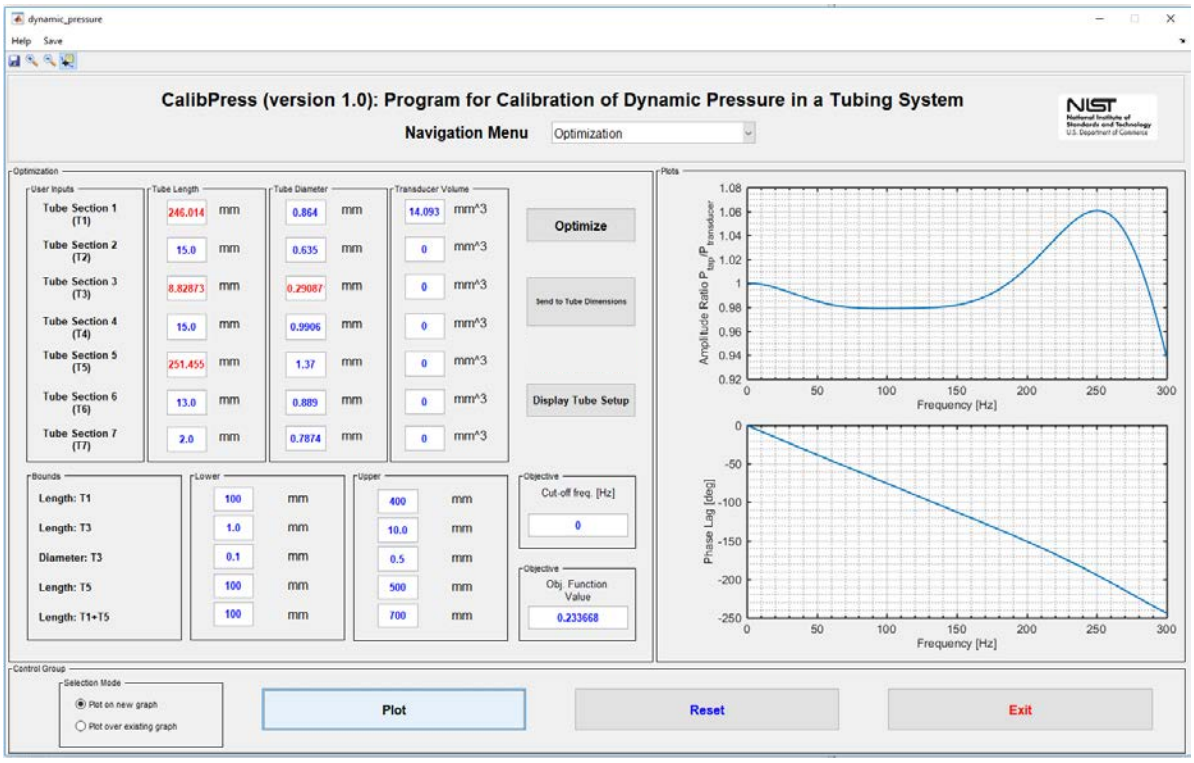

Figure 3.6 Screen-shot of optimization.

This publication is available free of charge from: https://doi.org/10.6028/NIST.TN.1994

4. EXPERIMENTAL MEASUREMENTS AND COMPARISONS

For the validation of the theoretical results, two tubes of different lengths were tested to measure the effects of the tubing system on the amplification or attenuation of pressure amplitudes and the shift of phase angle. Pressure time history data were generated across a wide range of pressure fluctuation frequencies by a wave generator. Based on the measured data, transfer functions for amplitude ratio and phase lag were created to calibrate the pressure data received from the pressure transducer through a tubing system.

4.1 Experimental Setup

An experimental device was developed for measurements of fluctuating pressures through tubing systems. As shown Figures 4.1 and 4.2, the device consists of (1) a wave function generator, (2) a wooden box including an air-tight room covered by a subwoofer speaker and a 30-mm thick acrylic plate, (3) six pressure taps through which air pressure can be transferred to tubing systems, (4) urethane tubes with inner diameters 0.86 mm and 1.37 mm, and (5) a pressure measurement system composed of a DSM4000 data-acquisition module and two ZOC33 miniature pressure scanners manufactured by Scanivalve. The pressure data were recorded on the hard drive using LabVIEW software by communicating with DSM4000 through an Ethernet connection.

The procedures for generating and measuring a sinusoidal pressure fluctuation with a specific frequency are as follows. A wave function generator sends a sinusoidal signal with a chosen frequency to a subwoofer attached to a wooden box. The speaker converts the sinusoidal electric signal with the specified frequency to a sinusoidal air pressure wave with the same frequency within the confined space consisting of the speaker and the acrylic plate. The pressure fluctuations are transferred to pressure taps connected to a tubing system. The air pressure signals on pressure taps connected to the one end of the tubing system are measured by the pressure measurement system connected to the system's other end. When fluctuating pressures are transferred through the tubing system, the amplitudes and phase angles of the pressure signals are distorted while the fluctuating frequency is unchanged. Thus, a calibration procedure for dynamic pressures measured via a tubing system is required, as shown in the following section.

This publication is available free of charge from: https://doi.org/10.6028/NIST.TN.1994

Figure 4.1. An experimental device for fluctuating pressure generation.

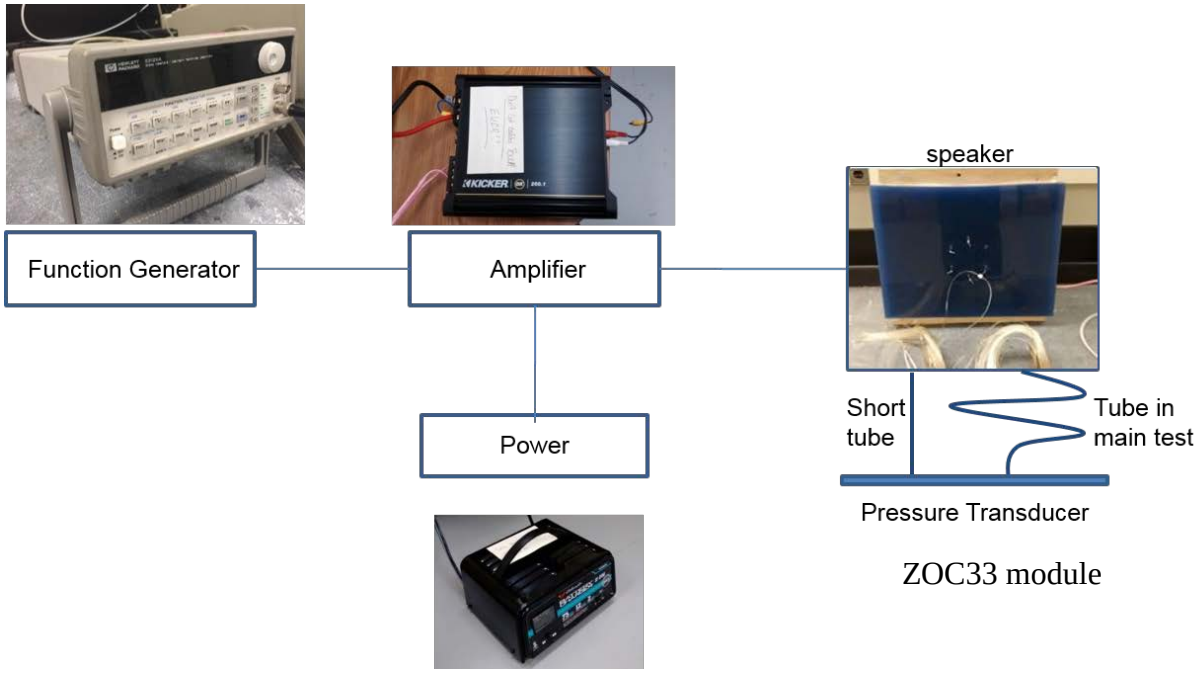

Figure 4.2. Experimental setup for data generation.

This publication is available free of charge from: https://doi.org/10.6028/NIST.TN.1994

4.2 Calibration Procedure

It was noted earlier that, as a pressure transducer cannot be directly attached to a pressure tap, a tubing system is employed for pressure measurement. As a result, the measured pressure data are distorted by a tubing system consisting of at least one tube. Depending upon the frequencies of the pressure signals, the amplitude and phase angles of the signals can be significantly changed. To address this problem, transfer functions for amplitude ratio and phase lag as functions of frequency are developed by using two different tubing systems. One system has a tube of very short length (e.g., usually less than 10 mm to 20 mm) for reference pressure signals. The other system consists of at least one long tube that will be used for experiments. For a given range of frequencies of interest, sinusoidal pressure signals corresponding to each frequency in increments of, say, 2 Hz are measured through the two tubing systems. At each frequency, amplitudes and phase angles of the measured pressure signals are calculated using the FFT (Fast Fourier Transform) algorithm in which the signals in the time domain, *p*, are converted to signals in the frequency domain, $P(n_k)$, corresponding to the *k*th frequency, as shown below (Mathworks 2016).

$$P(k) = \sum_{j=1}^{N} p(j) W_N^{(j-1)(k-1)} \tag{4.1}$$

where

$N =$ Number of samples

$W_N = e^{(-2\pi i)/N} =$ Complex *N*th root of unity.

The single-sided amplitude and phase angle at the *k*-th frequency, n_k, are then computed using the equations shown below:

$$amp(n_k) = \frac{2}{L} * |P(n_k)| \tag{4.2}$$

$$phase(n_k) = \tan^{-1}(P(n_k)) \tag{4.3}$$

where $L =$ length of signal.

The amplitude ratio of the two measured presure signals is then computed by dividing the amplitude of the long tube data for experiemntal use by the short reference tube data (Eq. 4.4).

$$A(n_k) = \frac{amp(n_k)_{long\ tube}}{amp(n_k)_{short\ tube}} \tag{4.4}$$

The phase lag from the long tube to the short tube can be calculated as the difference between the phase angles of the long tube and the short tube. If pressures are measured through multiple channels, additional phase lag can be generated by the method used to record pressures in the multi-channel transducer. In the system used in this study, pressures in 64 channels are recorded from the 1st channel to the 64th channel in order, which generates phase differences if the pressures in all channels are simultaneously taken into account. Equation 4.5 describes the phase lag due to the tubing system and the multi-channel measurement.

$$\phi_{lag}(n_k) = \phi(n_k)_{long\ tube} - \phi(n_k)_{short\ tube} - \Delta\phi(n_k)_{ch} \tag{4.5}$$

where $\Delta\phi(n_k)_{ch} = (2\pi\ \Delta ch\ n_k)/(64\ n_s)$; Δch is the difference between the number of the channel of interest and the number of the reference channel chosen from the total of 64 channels, n_s is the sampling frequency for pressure measurement. Based on the phase lags and the amplitude ratios over a chosen frequency range, two transfer functions can be generated for correcting signals.

4.3 Signal Correction Procedure

Let an experiment for pressure measurement be conducted by using the long tube. Because the measured pressure data are distorted by the tubing system, they need to be corrected by using the transfer functions obtained in the previous section. The first step for the signal correction procedure is to convert the pressure data from the time domain to the frequency domain. The measured pressure data in the frequency domain have a wide range of frequency components with distorted amplitudes and phase angles. Through the transfer functions, the amplitudes and phase angles can be corrected with respect to frequency. The requisite time-domain pressure data from which the tubing effects have been largely eliminated can be obtained by applying the discrete IFFT (Inverse Fast Fourier Transform) algorithm to the corrected amplitudes and phase angles (Mathworks 2016):

$$p(j) = \left(\frac{1}{N}\right)\sum_{k=1}^{N} P(n_k) W_N^{-(j-1)(k-1)}. \tag{4.6}$$

This publication is available free of charge from: https://doi.org/10.6028/NIST.TN.1994

This publication is available free of charge from: https://doi.org/10.6028/NIST.TN.1994

4.4 Case Study

A case study was considered wherein transfer functions obtained by the program developed in this study were validated experimentally. As described in Table 4.1, two types of tubing system were employed. The first system consisted of two long tubes with different diameters, connected by an adaptor (total length 350 mm, including the adaptor). The second system consisted of two short tubes, also connected by an adaptor (total length 70 mm, including the adaptor).

Table 4.1. Tubing configuration used for case study

		Pressure tap	Tube	Adaptor		Tube
Long Tube	Length [mm]	33	144	15	15	145.5
	Inner Diameter [mm]	0.889	1.37	0.991	0.635	0.86
Reference Tube	Length [mm]	33	2	15	15	3.5
	Inner Diameter [mm]	0.889	1.37	0.991	0.635	0.86

The tests were carried out over a frequency range of 30 Hz to 300Hz, determined by the frequency range of the speaker (27 Hz to 500 Hz) used in the experimental device, and the maximum sampling frequency (625 Hz) for pressure recording using the pressure measurement system. For data collection we started with the generated frequency at 30 Hz and increased the frequency by 2 Hz after each scan until we reached 300 Hz. We ran the pressure scanner at a sampling rate of 625 Hz and therefore kept the frequencies below the Nyquist frequency of 317.5 Hz (i.e., 625 Hz/2). The duration of each scan of the transducer was 30 s, and the time interval between consecutive scans was 30 s to allow stabilization of the pressure fluctuations with the changed frequency.

The collected data was then analyzed using the FFT to develop experimental transfer functions for the amplitude ratio and the phase lag. Theoretical transfer functions of the long tube and the reference tube were calculated using the program. To compare with the experimental transfer functions, the numerical transfer functions from two tubing systems were converted to one set of transfer functions for amplitude ratio and phase lag by dividing the amplitude ratio transfer functions for the long tube by its counterpart for the reference tube, and by subtracting the phase lag of the reference tube from the phase lag of the long tube, respectively. This set of transfer functions is equivalent to the transfer functions yielded by the experiment. The comparison between the theoretical and the experimental data is then performed as shown in the following section.

This publication is available free of charge from: https://doi.org/10.6028/NIST.TN.1994

4.5 Comparison of Theoretical and Experimental Data

Figure 4.3 shows that the differences between the experimental and numerical transfer functions are small. Note that the experiment data in the figure are the average values in three trials.

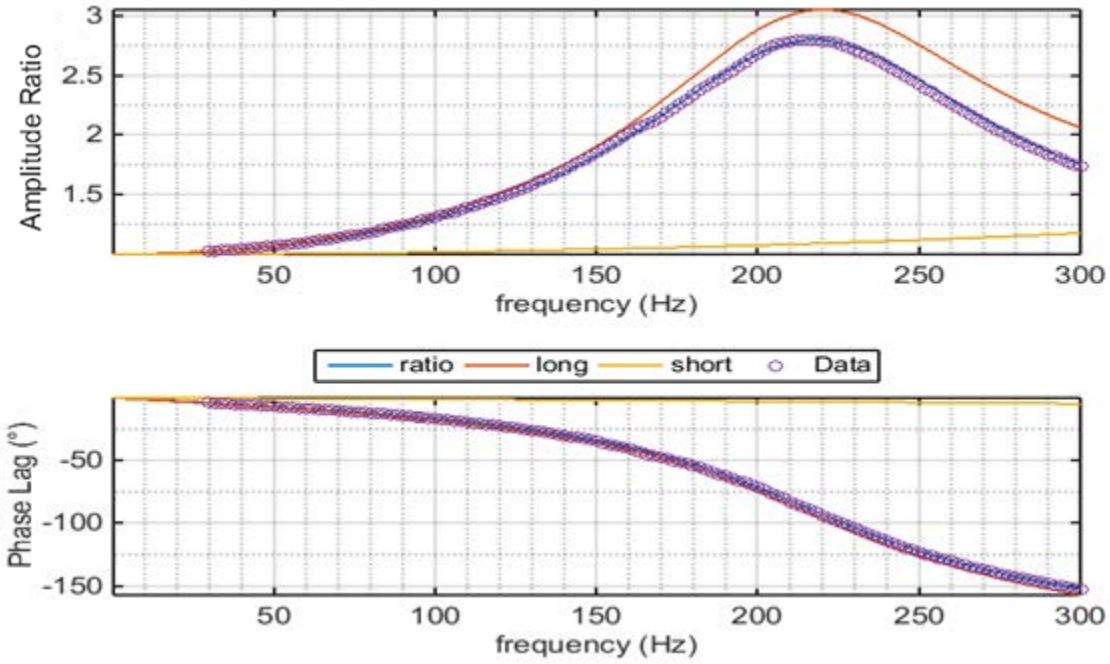

Figure 4.3. Experimental comparison to theoretical prediction for the behavior in the tubing systems.

Figure 4.4 shows errors between experimental and numerical data. The upper plot presents relative errors of amplitude ratios obtained in experimental and numerical approaches. The error bar at each frequency indicates the standard deviation of three experimental results above and below their average. As shown in the plot, the errors within the frequency range of interest are less than ± 3%. The lower plot uses absolute errors of phase lag between both approaches, since the differences of phase angle in trigonometric functions play an important role. The errors are less than approximately 6 degrees while they decrease at low frequencies.

This publication is available free of charge from: https://doi.org/10.6028/NIST.TN.1994

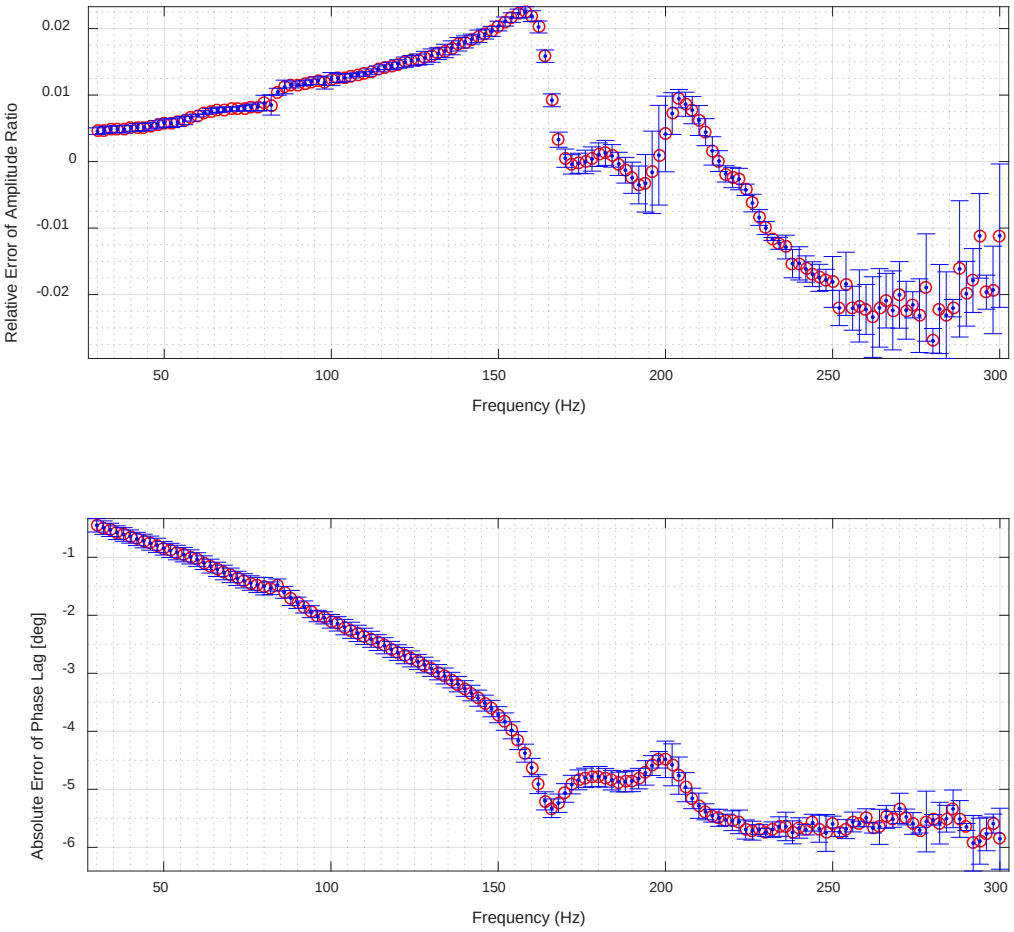

Figure 4.4. Errors in amplitude ratios (top) and phase lags (bottom) between numerical and experimental approach.

4.6 Comparison of Data from Two Theoretical Models

For validation of the theoretical model used in this study, a lumped-element transmission line model is employed. The model is based on acoustic propagation in tubes. For details see Appendix B. The study assumes 20℃ dry air of nitrogen in a 1 m long tube whose diameter is 0.86 mm under atmospheric pressure of 101325 Pa.

Figure 4.5 shows relative errors of amplitude ratios and absolute errors of phase lags from two theoretical models used in the study and described in Appendix, respectively. The plots show at most approximately 1% relative error in amplitude ratios and 0.4 degree absolute error in phase lag, which confirms again that the program developed in this study can provide an accurate calibration procedure for fluctuating pressure measured via a tubing system.

This publication is available free of charge from: https://doi.org/10.6028/NIST.TN.1994

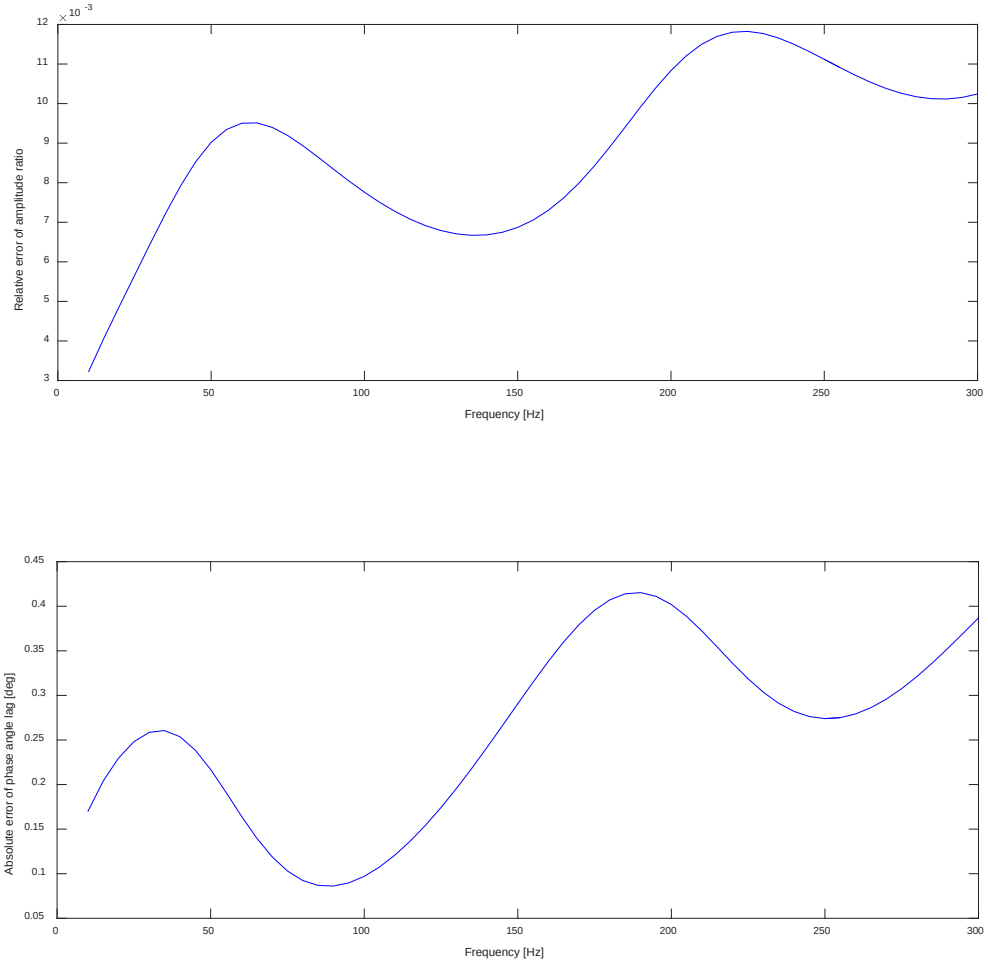

Figure 4.5. Errors in amplitude ratios (top) and phase lags (bottom) between two theoretical models

This publication is available free of charge from: https://doi.org/10.6028/NIST.TN.1994

5. PARAMETERS AFFECTING MEASURED PRESSURES

5.1 Effects of Tube Lengths

Effects of tube lengths on transfer functions were examined in a simple system of one tube and one volume of 14.093 mm^3, as shown in Figure 5.1.

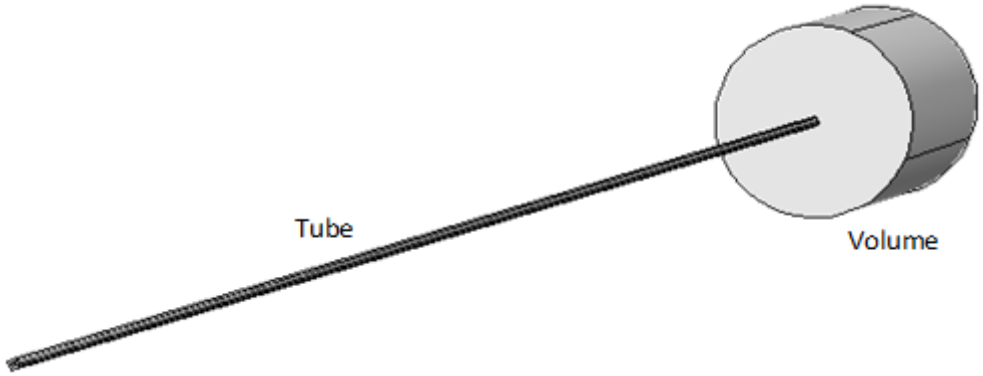

Figure 5.1. Tube system of one tube and one volume

Figure 5.2 shows the effects of varying the length of a tube from 0.1 m to 1.1 m. As expected, the shortest tube length gives the best performance with amplification increasing up to 1.4 at 300 Hz. The tube lengths up to 0.3 m result in an increase of the maximum amplitude ratio at higher frequencies. The tube lengths of 0.5 m and longer tend to reduce the maximum value and to attenuate the amplitudes. All variables other than the length were kept constant. These variables are listed in Table 5.1.

This publication is available free of charge from: https://doi.org/10.6028/NIST.TN.1994

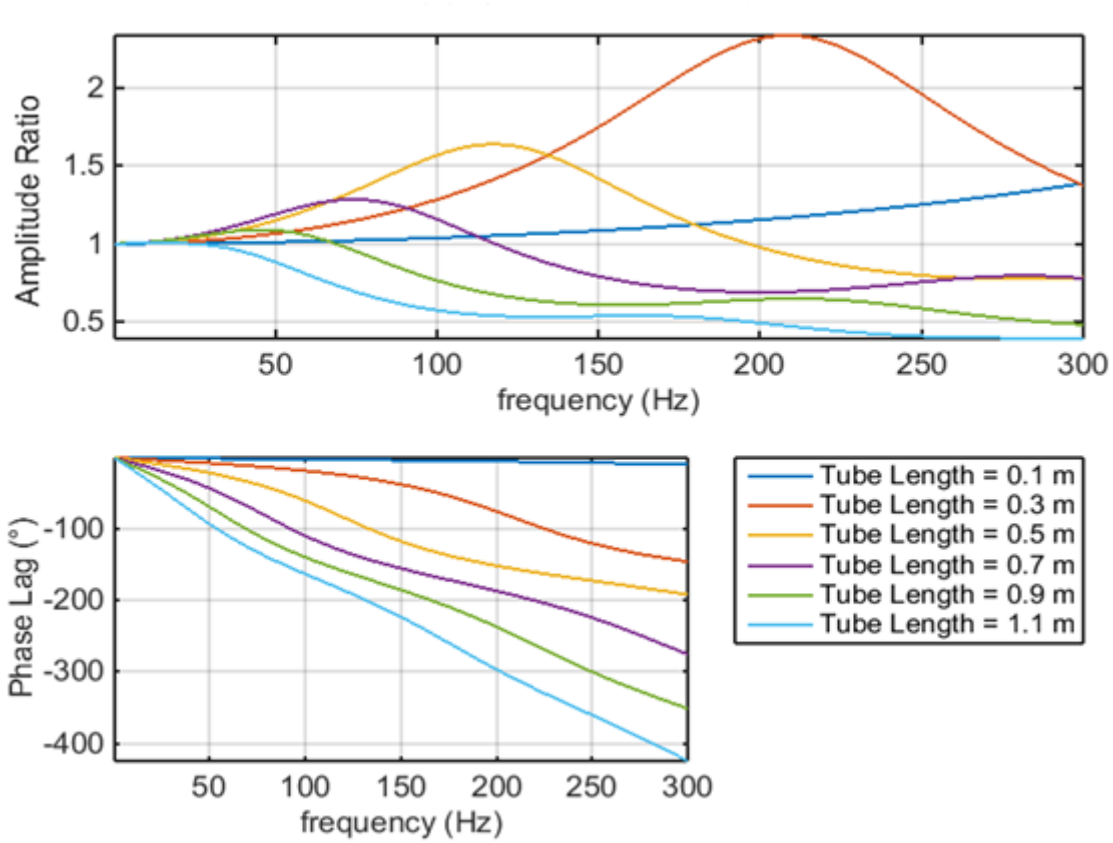

Figure 5.2. Effect of the variation of tube length

Table 5.1. Properties of tube system seen in Figure 5.2

Tube Diameter	0.86	mm
Temperature	20	℃
Pressure	101325	Pa
Relative Humidity	0	%

This publication is available free of charge from: https://doi.org/10.6028/NIST.TN.1994

5.2 Effect of Tube Diameters

The effect of the variation of the tube diameter was explored for the case where the tube length was 0.5 m. The diameter was varied from 0.1 mm to 1.1 mm. Figure 5.3 illustrates the effect of these variations. Smaller diameter tubes cause excessive amplitude attenuation, while large diameter tubes cause signal amplification. The constant variables for this test are shown in Table 5.2.

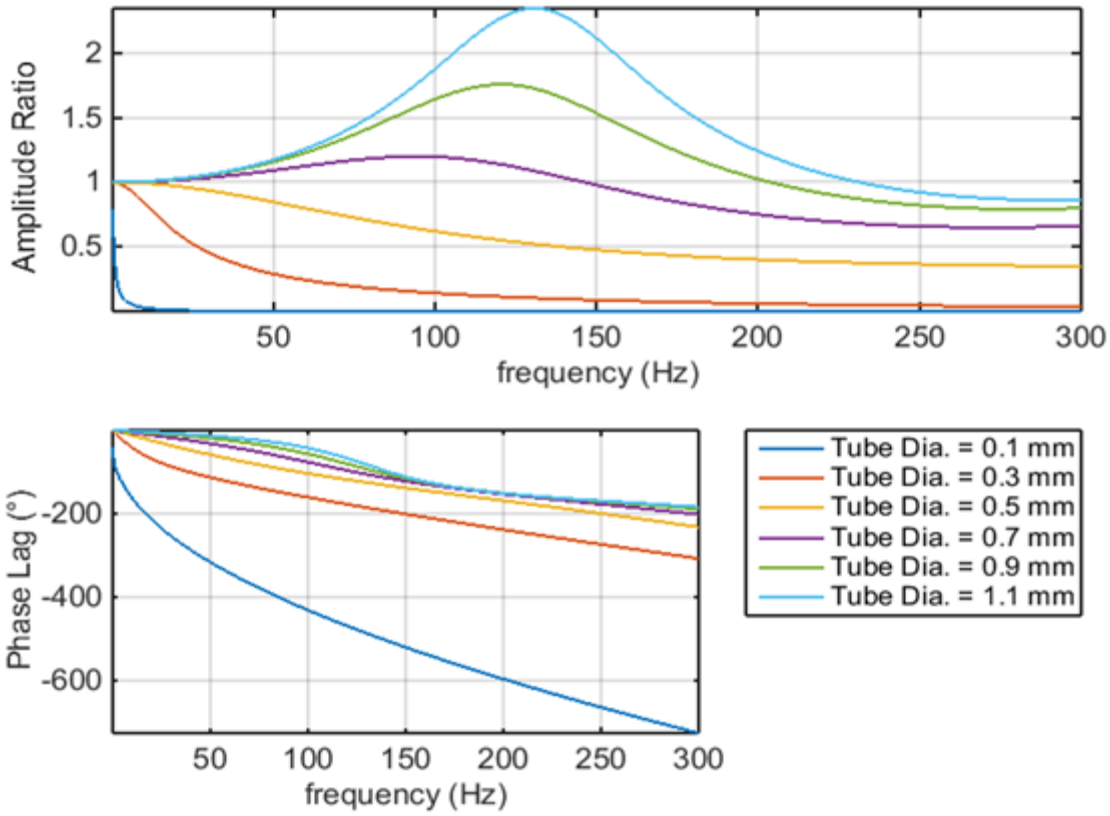

Figure 5.3. Effect of variation of tube diameter. So which diameter would one choose?

Table 5.2. Properties of tube system seen in Figure 5.3

Tube Length	500	mm
Temperature	20	℃
Pressure	101325	Pa
Relative Humidity	0	%

This publication is available free of charge from: https://doi.org/10.6028/NIST.TN.1994

5.3 Effects of Temperature, Atmospheric Pressures, and Humidity

The effects of temperature and pressure variation were also examined. The variation of these properties will affect the secondary variables that are calculated through the use of the Equation of State. First, the effects of temperature were considered. The temperature was varied form 15 ˚C to 40 ˚C. The effects are shown in Figure 5.4. The trend for these variations show that lower temperatures yield augmented amplitude responses. These tests were performed with the constant variables shown in Table 5.3.

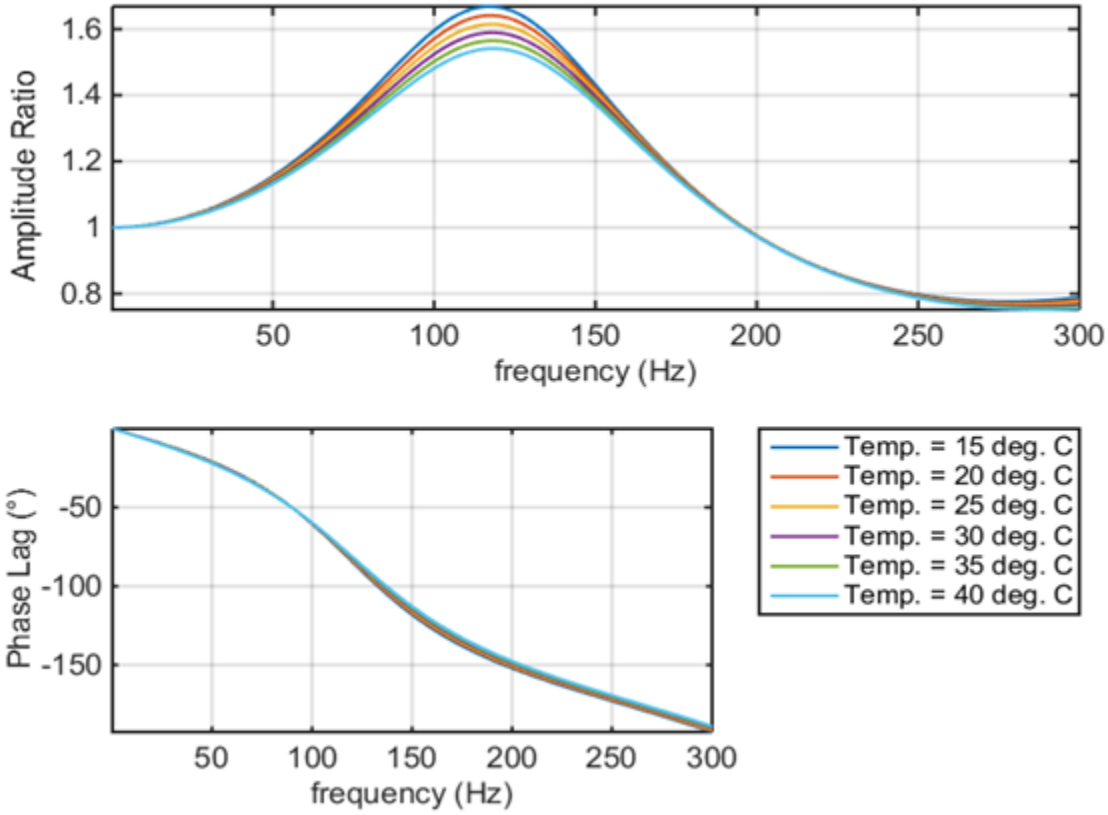

Figure 5.4. Effects of the variation of temperature.

Table 5.3. Properties of tube system seen in Figure 5.4

Tube Length	500	mm
Tube Diameter	0.86	mm
Pressure	101325	Pa
Relative Humidity	0	%

This publication is available free of charge from: https://doi.org/10.6028/NIST.TN.1994

Figure 5.5 shows the effects of atmospheric pressure on the transfer functions. It is seen that higher atmospheric pressures increase the amplitudes more strongly than lower pressures do. The properties of the tube system used in this case are summarized in Table 5.4.

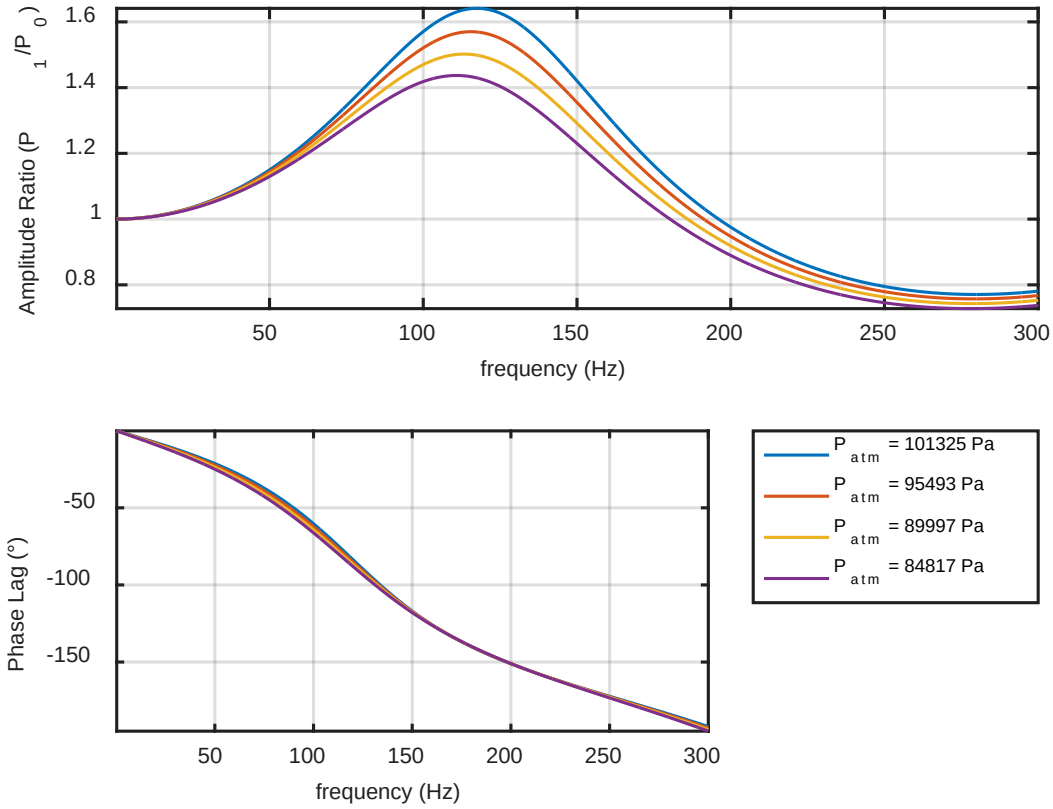

Figure 5.5. Effects of atmospheric pressure.

Table 5.4. Properties of tube system seen in Figure 5.5

Tube Length	500	mm
Tube Diameter	0.86	mm
Temperature	20	℃
Relative Humidity	0	%

Effects of relative humidity were also investigated. The results show that the effects of relative humidity are less than 1 % between relative humidity of 0 % and 50 %, in the case of the simple system with 500 mm length and 0.86 mm. The temperature and pressures used in the study were 20 °C and 101325 Pa.

This publication is available free of charge from: https://doi.org/10.6028/NIST.TN.1994

6. OPTIMIZATION OF TUBING SYSTEMS

6.1 Minimization of Tubing Effects on Pressure Measurements

Once the numerical approach was approved for its performance after validation with the experimental results, a tubing system can be designed by the program to obtain a better transfer function. It is widely known that a restrictor significantly reduces the tubing effects. Thus we investigated the configuration of a tubing system including a restrictor to minimize the acoustic and visco-thermal effects of the fluid media, as well as the effects of the boundary layer and the tubing material structure and dimensions. An extensive work on the optimization was performed by Holmes and Lewis (1987a; 1987b). From the work of Irwin et al. (1979), it was found that for tubing systems of up to two feet in length, which showed small phase distortion, pressure regulation remained well managed by the use of a restrictor. As the tubing system in this situation was much less than two feet, it was decided to make use of a restrictor. From comparisons with experiment it was found that the recursion formula (Eq. 2.3) predicted very accurately the behavior of the fluid inside the confines of a tubing system. However, due to the uniqueness of each situation, no simple solution existed for the use of the requisite restrictor. With this limitation in mind, it was decided to modify the program to allow for the optimization of the dimensions of the tubing system. In this study a MATLAB optimization function, fmincon, was used. This function allows for minimization of constrained functions using selected algorithms. To obtain the optimized configuration for minimization of tube effects on the transfer functions, the objective function was set as shown in Eq. 6.1. This function uses the pressure amplitude ratio data from each iteration of the program and performs a search to identify the maximum and minimum values. The absolute value of the difference was used as the objective. The constraints were imposed upon the tubing system were related to the model construction, the available tubes, and the pressure transducer itself.

The following objective function f_{OBJ} is employed in this study:

$$f_{OBJ} = \min\left[W(n) \int_0^{n_{\max}} (|R_p| - 1)^2 \, dn \right] \tag{6.1}$$

where

R_p = Amplitude ratio of pressure data as a function of frequency (defined in Eq. 2.1)

$W(n)$ = Weight function as a function of frequency.

The weight function has two options: unity or hyperbolic tangential function values between 0 and 1, over the frequency range:

$$W(n) = \begin{cases} 1 & \text{or} \\ \frac{1}{2}\tanh\left(-\frac{n-n_c}{n_c/5}\right)+\frac{1}{2}, & n_c = \text{threshold frequency for weights.} \end{cases} \quad (6.2)$$

While the former function has the same weight over the frequency range, the latter enables to provide more weight in a low frequency range than in a higher frequency range by controlling the threshold frequency, n_c whose weight value is, for example, 0.5 as shown in Fig. 6.1.

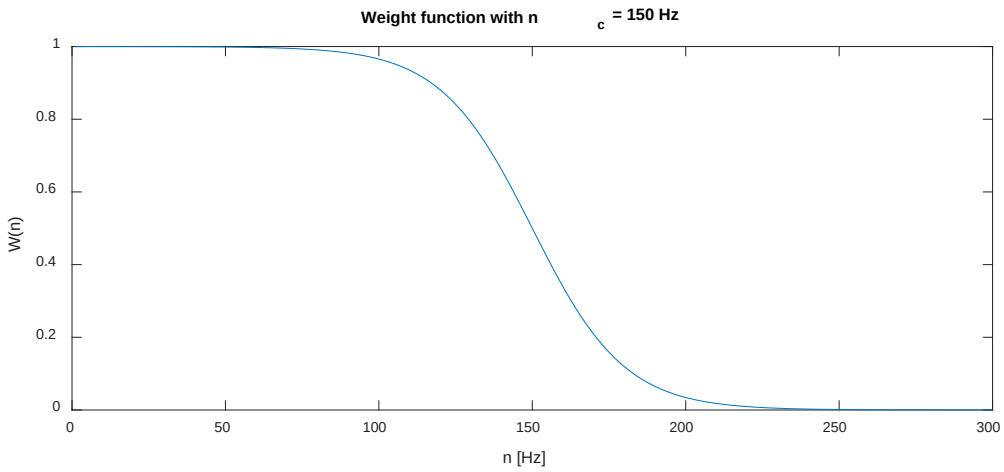

Figure 6.1 Weight function with threshold frequency of 150 Hz.

This publication is available free of charge from: https://doi.org/10.6028/NIST.TN.1994

This publication is available free of charge from: https://doi.org/10.6028/NIST.TN.1994

6.2 Model Size and Configuration Limitations

The limitations of the wind tunnel model need to be considered in order to determine the dimensions of the tube system, fittings, and transducer for a single pressure tap. Figure 6.2 shows the geometry of the rectangular cylinder model to be used in wind tunnel testing.

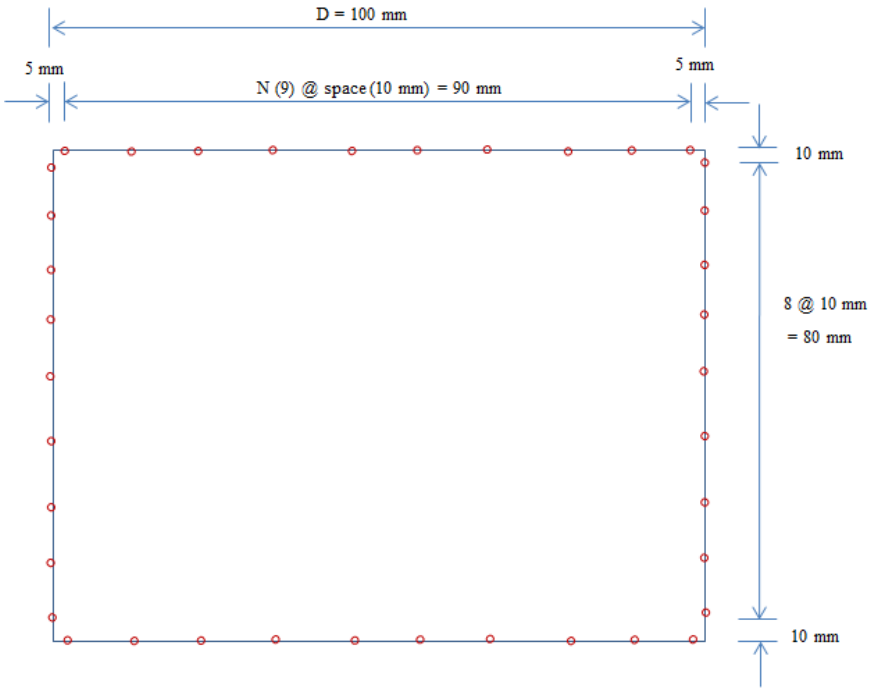

Figure 6.2 Cross-section of a square cylinder model
(the circles shows the positions of pressure taps).

The tap placement on the four faces of the cylinder is summarized in Table 6.1.

Table 6.1. Outer cylinder tap information

Windward wall	9/row x 10 rows = 90
Upper Wall	10/row x 10 rows = 100
Leeward Wall	9/row x 10 rows = 90
Lower Wall	10/row x 10 rows = 100
Sum of Taps	380

Figure 6.3 illustrates the placement of the pressure transducer array and other interior features of the model.

This publication is available free of charge from: https://doi.org/10.6028/NIST.TN.1994

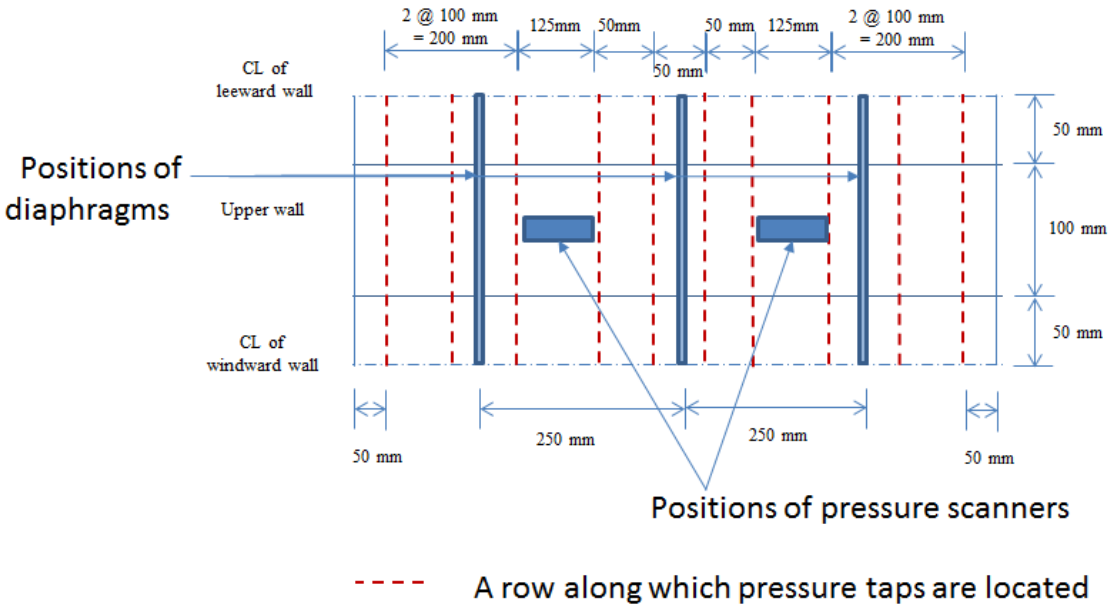

Figure 6.3 Upper cross-section of model.

Figure 6.4 shows details of pressure taps installed on the plexiglass wall of the model. To keep the tap length constant (i.e., 13 mm), the embedded lengths of the tap in the plexiglass walls vary depending on the thickness of the wall. Holes from the outside wall surface to the pressure taps are 2 mm in length and 0.787 mm in diameter. Aerodynamic pressures propagate through the hole and the pressure tap and subsequently to a pressure sensor of the pressure scanner.

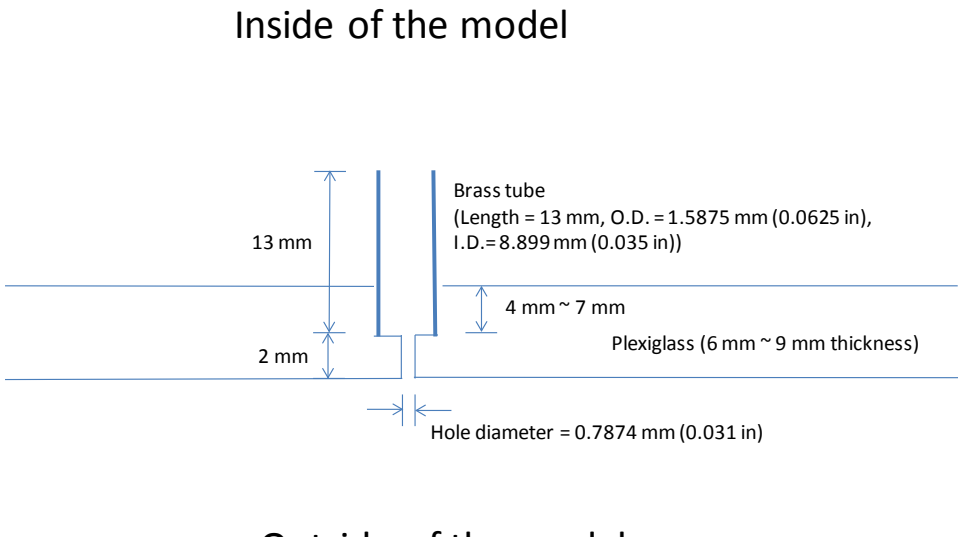

Figure 6.4 A section of the model wall showing a pressure tap.

This publication is available free of charge from: https://doi.org/10.6028/NIST.TN.1994

Due to the different diameters of the pressure tap on the model and the sensor tap of the pressure scanner, the minimum number of tube sections is three, counting a fitting tube (i.e., a reducer or an adaptor) from the pressure tap to the pressure transducer. Thus, the unknown values in the tubing system are the lengths of Tubes 1 and 2, as shown in Table 6.2. It was assumed that tests would be performed for the possible range of temperature in a wind tunnel facility (i.e., 15˚C to 28˚C) and atmosphere pressure of 101325 Pa with a relative humidity of 40%.

Table 6.2. Constants and unknown values of tubing system of six components

Variable	Measured Dimension	Value	Unit
Transducer	Volume	14.093	mm^3
Tube 1	Interior Diameter	0.86	mm
	Length	unknown	mm
Fitting-Tube 1 side	Interior Diameter	0.635	mm
	Length	15.0	mm
Fitting-Tube 2 side	Diameter	0.9906	mm
	Length	15.0	mm
Tube 2	Diameter	1.37	mm
	Length	unknown	mm
Tap Adapter	Diameter	0.889	mm
	Length	13.0	mm
Tap	Diameter	0.7874	mm
	Length	2.0	mm

The optimization calculations resulted in the following: 200 mm long Tube 1 and 100 mm long Tube 2 for the best performance of the tubing system 2 (Table 6.3). As shown in Figure 6.4, the optimized objective function yielded a value of 1.6804.

Table 6.3. Optimized values of tube lengths

Variable	Measured Dimension	Value	Units
Tube 1	Length	200	mm
Tube 2	Length	100	mm

.

This publication is available free of charge from: https://doi.org/10.6028/NIST.TN.1994

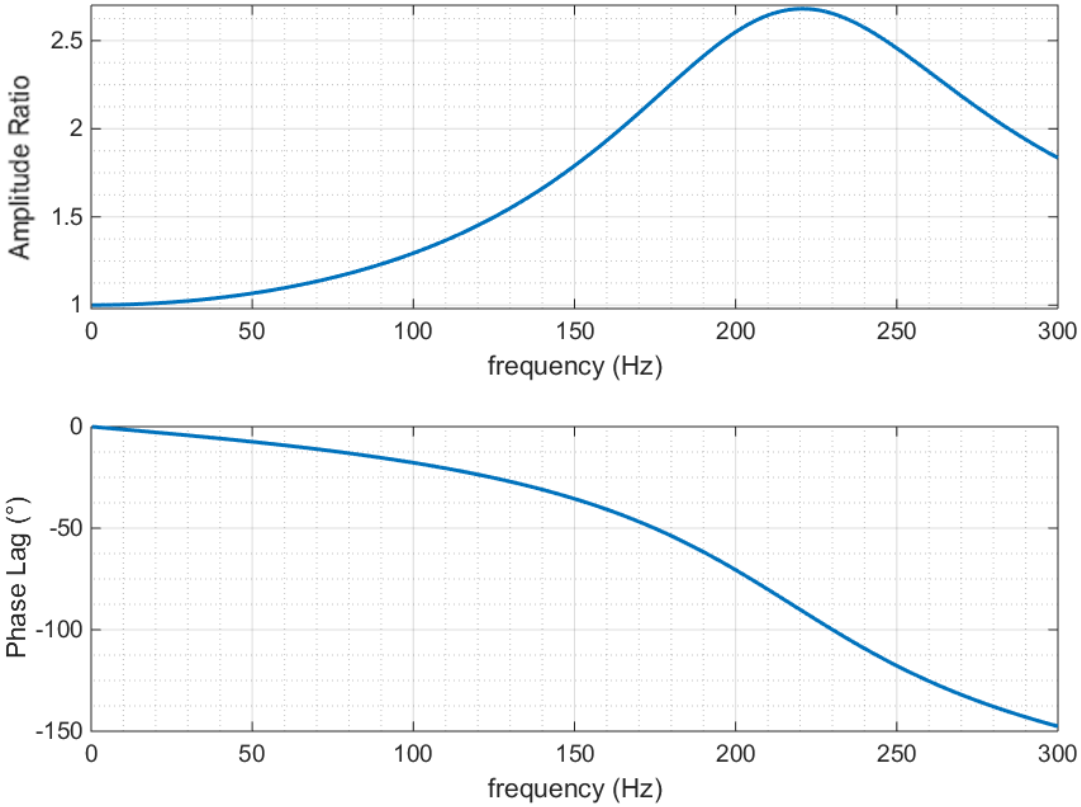

Figure 6.5 Plot of amplitude ratio and phase lag for the simple tubing configuration.

For better performance of transfer functions in a tubing system, it was suggested that a restrictor be installed in the middle of the reducer. This restrictor fitting was expected to attenuate the amplitude change and yield a value of amplitude ratio that is consistently close to unity. The configuration of this tubing system is described in Table 6.4. In addition to unknown lengths of Tubes 1 and 2, the inner diameter and the length of the restrictor need to be determined in this optimization problem. The optimized values for the unknowns are shown in Table 6.5. As shown in Figure 6.6, the performance of transfer functions is significantly improved in comparison with the performance of the earlier simple tubing system. The optimized objective value for this tubing system was smaller by two orders of magnitude than for the system without a restrictor. The value of the amplitude ratio can be seen to be close to unity and the phase angle is linear throughout the progression of the signal.

Table 6.4. Constants and unknown values of tubing system of seven components

Variable	Measured Dimension	Value	Units
Transducer	Volume	14.093	mm^3
Tube 1 (URTH-040)	Interior Diameter	0.864	mm
	Length	unknown	mm
Fitting-Tube 1 side	Interior Diameter	0.762	mm
	Length	14.0	mm
Fitting-Restrictor	Interior Diameter	unknown	mm
	Length	unknown	mm
Fitting-Tube 2 side	Diameter	0.9906	mm
	Length	14.2	mm
Tube 2 (URTH-063)	Diameter	1.372	mm
	Length	unknown	mm
Tap Adapter	Diameter	0.889	mm
	Length	13.0	mm
Tap	Diameter	0.7874	mm
	Length	2.0	mm

Table 6.5.Optimized values of tube lengths and diameter

Variable	Measured Dimension	Value	Units
Tube 1 (URTH-040)	Length	176.7	mm
Fitting-Restrictor	Interior Diameter	0.2233	mm
	Length	2.9	mm
Tube 2 (URTH-063)	Length	141.5	mm

This publication is available free of charge from: https://doi.org/10.6028/NIST.TN.1994

This publication is available free of charge from: https://doi.org/10.6028/NIST.TN.1994

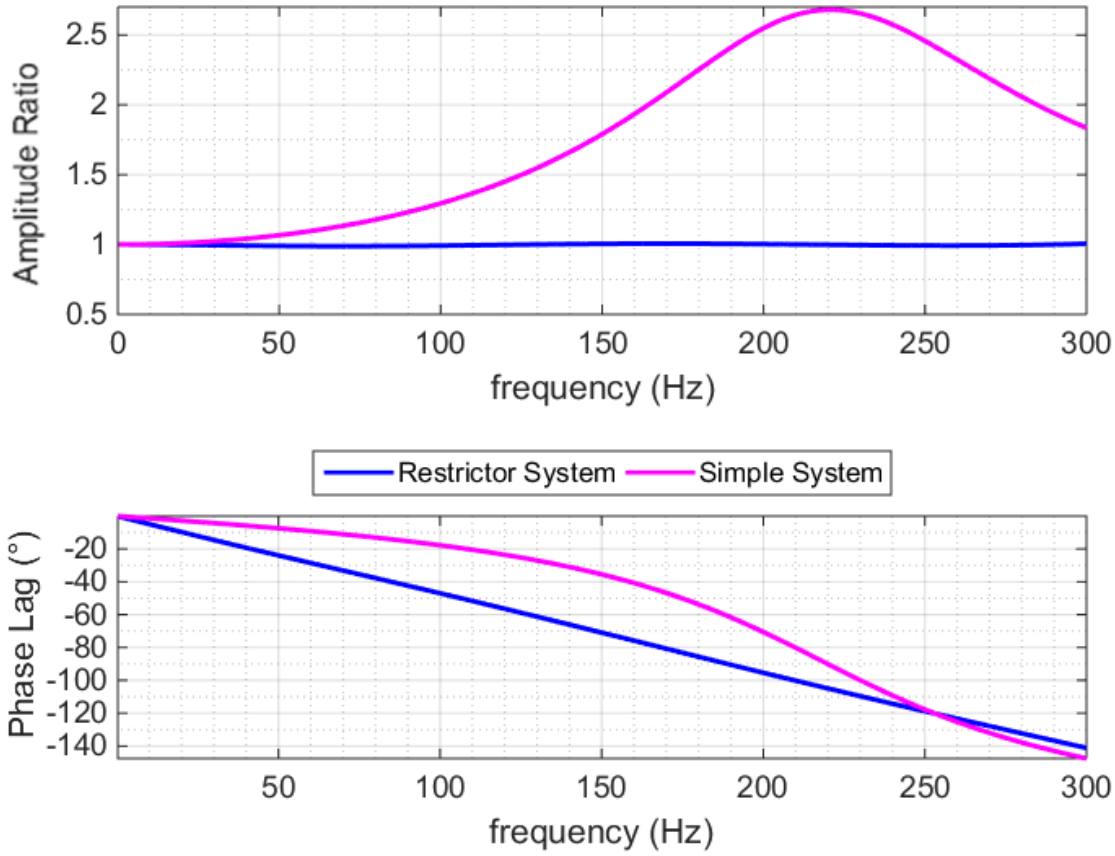

Figure 6.6 Plot of amplitude ratio and phase lag for the tubing configuration with a restrictor.

The performance of the tubing system with a restrictor was investigated for the possible range of temperature in a wind tunnel facility (i.e., 15˚C to 28˚C). As shown in Figure 6.7, the change in transfer functions is negligible over this temperature range.

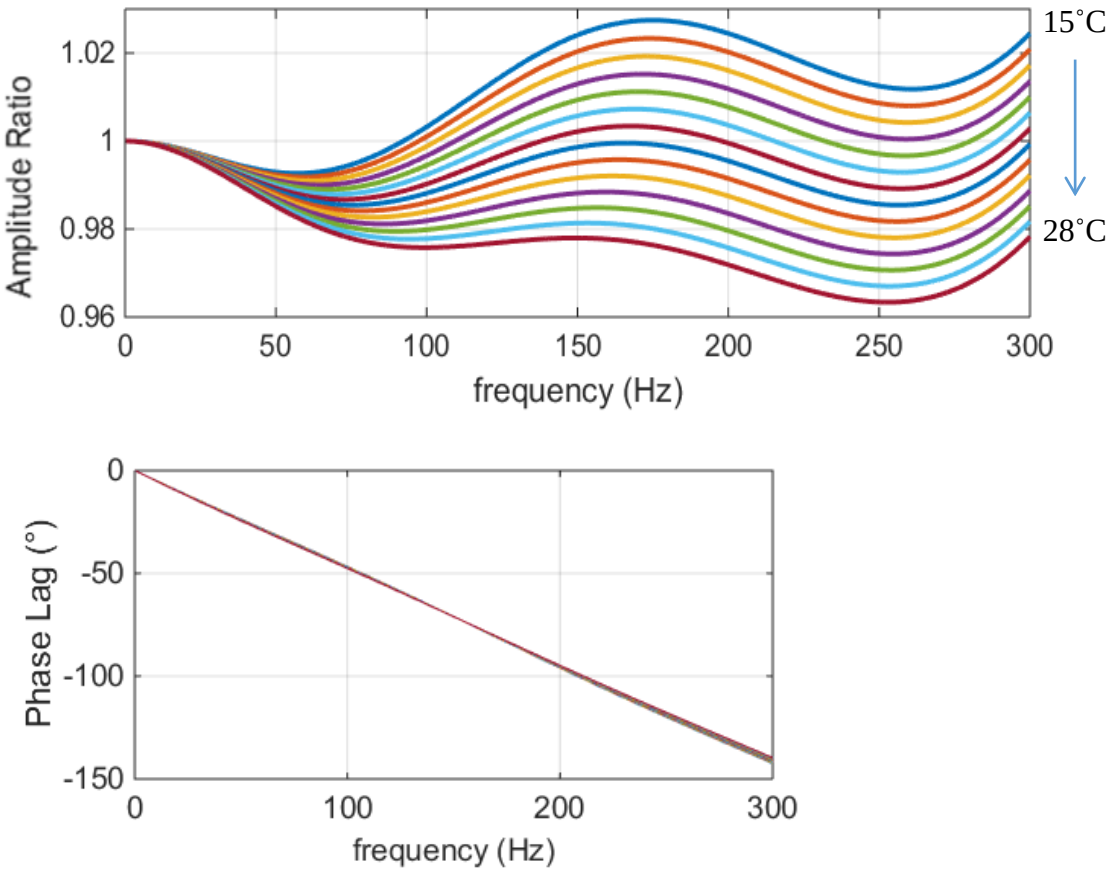

Figure 6.7 Plot over a range of temperatures from 15 ˚C to 28˚C with mean value restrictor data.

This publication is available free of charge from: https://doi.org/10.6028/NIST.TN.1994

This publication is available free of charge from: https://doi.org/10.6028/NIST.TN.1994

6.3 Experiments of Performance in the Designed Tubing System with a Restrictor

Figure 6.8 shows a restrictor built for experiments, based on the design of the optimized tubing system mentioned in the previous section (Tables 6.4-5). For an experimental investigation of the performance in the tubing system, the restrictor was connected to the fluctuating pressure-generating device explained in Section 4.1. A fluctuating pressure signal generated by a speaker was measured in the pressure scanner through the designed tubing system and a short reference tubing system shown in Table 4.1. Figure 6.9 shows the transfer functions of amplitude ratios and phase angle differences for dynamic pressures between the designed tube and the reference tube as a function of frequency of fluctuating pressure signals. The solid line represents numerical results calculated by the program developed in this study. The circles denote experimental results averaged from five tests and the error bars from the circles illustrate their positive and negative standard deviations, which are not clearly shown due to the small values. The differences of less than 3 % between both experiment and program confirm that the designed tubing system with a restrictor will significantly reduce the tubing effects on measurement of fluctuating pressure signals in pressure-measuring experiments using a tubing system.

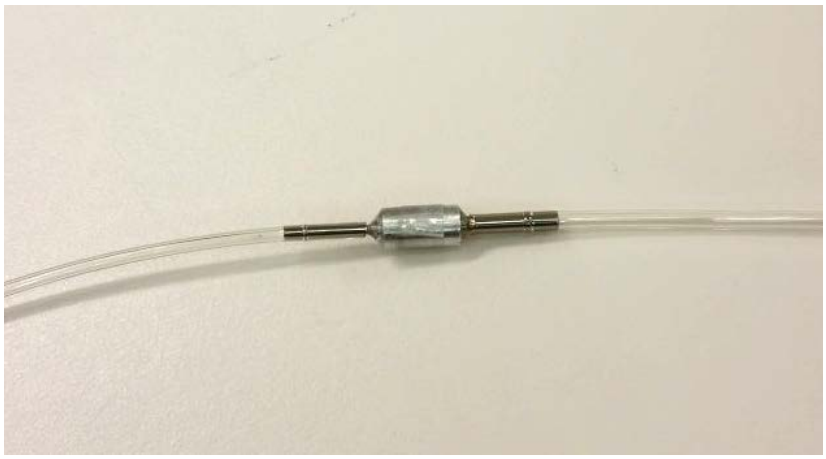

Figure 6.8 Restrictor built for experiments.

This publication is available free of charge from: https://doi.org/10.6028/NIST.TN.1994

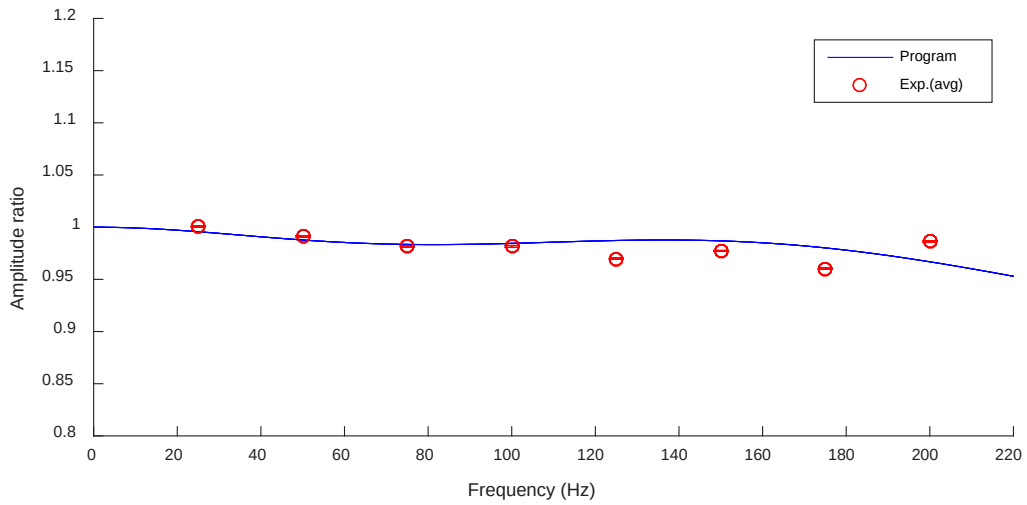

(a) Amplitude ratios

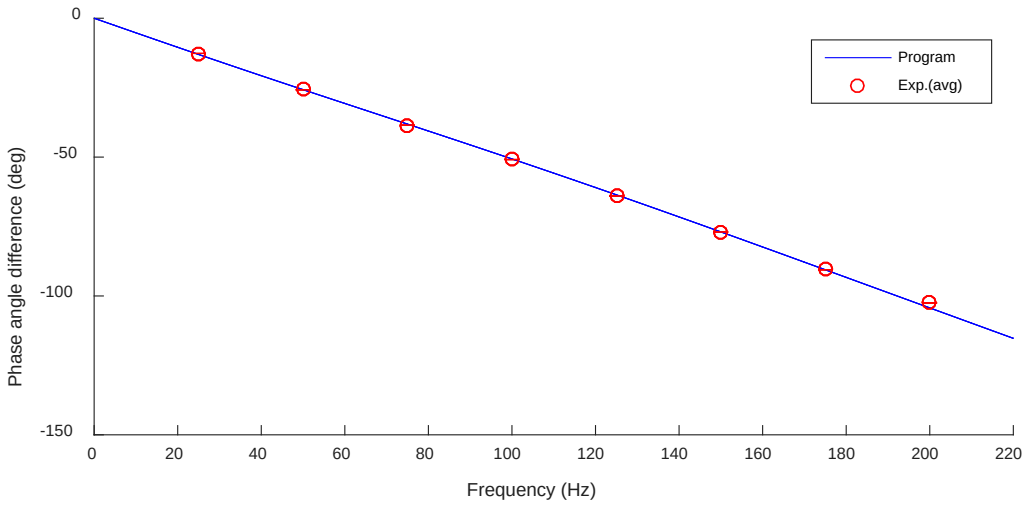

(b) Phase angle differences

Figure 6.9 Comparison of transfer functions from experimental and numerical data

This publication is available free of charge from: https://doi.org/10.6028/NIST.TN.1994

7. CONCLUSIONS

For accurate measurements of pressures on a building model in wind tunnel tests, we developed numerical and experimental approaches to calibrate the pressure data measured via a tubing system. The numerical approach employed the Navier-Stokes Equations, expressions for thermodynamic behavior and wave propagation, and mass and energy conservation equations for a sinusoidal motion of air in a cylindrical tubing system. We developed a MATLAB-based program *CalibPress* (version 1.0) to calculate the transfer functions for amplitude ratios and phase lags as functions of the frequency of pressure fluctuations in a given tubing configuration. The program also used REFPROP software developed by NIST to obtain the requisite air properties.

To validate the theoretical model used in the program developed in this study, two methods were employed: an experimental method using a function generator, a speaker system, and a theoretical method based on the lumped-element transmission line model. The results obtained by both methods showed that the program developed in this study can achieve an accurate calibration.

Effects of parameter values on measured pressures were investigated. The parameters used in this study include not only tube dimensions (i.e., tube length and inner diameters) but also air properties (i.e., temperature, atmospheric pressure, and relative humidity). The results showed that the environmental parameters of atmospheric pressure and temperature can influence significantly the pressures measured in a tubing system, which should be corrected for the accurate pressure measurement. A forthcoming study will be devoted to the effect on the pressure data of (i) the phase angle change due to the tubing system, and (ii) the environmental parameters, including the atmospheric pressure and the air temperature.

An optimization design procedure of a typical tubing system was developed for designed and tested for minimization of tubing effects on pressure measurements.

REFERENCES

ASTM (2015). *Standard Test Method for Measuring Humidity with a Psychrometer* (*the Measurement of Wet- and Dry-Bulb Temperatures*), E337-15, ASTM International, West Conshohocken, PA.

Bergh, H. and Tijdeman, H. (1965). *Theoretical and experimental results for the dynamic response of pressure measuring systems*. Rep. NLR-TR F.238.

Elson, J.P. and Soedel, W. (1972). "Criteria for the design of pressure transducer adapter systems." *International Compressor Engineering Conference*. 390-394.

Holmes, J. D., and Lewis, R. E. (1987a). "Optimization of dynamic-pressure-measurement systems. I. Single point measurements." *Journal of Wind Engineering and Industrial Aerodynamics*, 25(3), 249-273.

Holmes, J. D., and Lewis, R. E. (1987b). "Optimization of dynamic-pressure-measurement systems. II. Parallel tube-manifold systems." *Journal of Wind Engineering and Industrial Aerodynamics*, 25(3), 275-290.

Irwin, H. P. A. H., Cooper, K. R., and Girard, R. (1979). "Correction of distortion effects caused by tubing systems in measurements of fluctuating pressures." *Journal of Wind Engineering and Industrial Aerodynamics*, 5(1), 93-107.

Lemmon, E. W. and Huber, M. L. (2015). *NIST Reference Fluid Thermodynamic and Transport Properties Database (REFPROP): Version 9.1.*, National Institute of Standards and Technology, http://www.nist.gov/srd/nist23.cfm.

Mathworks (2016). "MATLAB, version 9.1.0 (R2016b)." Natick, MA, USA.

This publication is available free of charge from: https://doi.org/10.6028/NIST.TN.1994

This publication is available free of charge from: https://doi.org/10.6028/NIST.TN.1994

APPENDIX A

DETERMINATION OF RELATIVE HUMIDITY IN HUMID AIR

Once the expressions for the calculation of the dry air properties are defined, a method is needed to accurately estimate the amount of water vapor in the air. Relative humidity can be translated into mole fraction of water vapor in the air, which is relatively easy to measure. However, REFPROP only has a built-in value for dry air consisting of Nitrogen, Oxygen, and Argon. For the case of humid air, the program also accounts for Carbon Dioxide in addition to the three main components, as shown in Table A.1.

Table.A.1. Composition of air assumed in the program

Component	Mole Fraction
Nitrogen	0.7812
Oxygen	0.2096
Argon	0.0092
Carbon Dioxide	0.000383
Total	1.0000

In most cases air cannot be treated as a completely dry gas. It typically contains a certain amount of water vapor, called the absolute humidity.

The relative humidity can be defined using mole fractions or pressures of water vapor and saturated water vapor under the ideal gas assumption [1]:

$$\mathrm{RH} = \frac{x_{H_2O}}{x_{sH_2O}} = \frac{p_{a,H_2O}}{p_{s,H_2O}} \tag{A.1}$$

[1] Perry, Robert H., Don W. Green, and James O. Maloney (1984). *Perry's Chemical Engineers' Handbook*. 8th ed. New York: McGraw-Hill.

where

x_{H_2O} = the mole fraction of water vapor
x_{sH_2O} = the mole fraction of saturated water vapor
p_{a,H_2O} = the partial pressure of water vapor
p_{s,H_2O} = the pressure of saturated water vapor.

This ratio can be also related to the mole fraction of water vapor through the following relationship:

$$x_{H_2O} = \frac{n_{H_2O}}{n_T} = \frac{p_{a,H_2O}}{p_T} \tag{A.2}$$

where

n_{H_2O} = the number of moles of water vapor
n_T = the total number of moles in mixture
p_T = the total atmospheric pressure.

Because the interaction between real gas molecules increase a small amount of the saturated vapor pressure in air, an enhanced factor $f(p,T)$ is adopted to correct the mole fraction of saturated water vapor (Eqs. A.1 and A.2) as described below:

$$x_{sH_2O} = f(p,T)\frac{p_{s,H_2O}}{p_T} \tag{A.3}$$

where the enhanced factor $f(p,T)$ is a function of ambient pressure p and temperature T [2].

$$f(p,T) = e^{\left[\xi_1\left(1-\frac{p_{s,H_2O}}{p_T}\right)+\xi_2\left(\frac{p_{s,H_2O}}{p_T}-1\right)\right]}. \tag{A.4}$$

[2] Tsilingiris, P. T. (2008). "Thermophysical and transport properties of humid air at temperature range between 0 and 100 °C." *Energy Conversion and Management*, 49(5), 1098-1110.

This publication is available free of charge from: https://doi.org/10.6028/NIST.TN.1994

In the equation above

$$\xi_1 = \sum_{i=0}^{3} A_i \, T^i$$

$$\xi_2 = \exp\left(\sum_{i=0}^{3} B_i \, T^i\right)$$

$A_i, B_i =$ numerical fitting constants for water.

A simple and relatively accurate method to measure relative humidity is included in ASTM E337-15 [3]based on psychrometric hygrometry. Equation (A.5) can calculate the relative humidity measured with a psychrometer under the assumption that the barometer pressure is equal to 101325 Pa. This will determine the value of relative humidity to within a 95% confidence level [3]:

$$RH_o = \frac{p_{s,T_w} - A\, p_T (T_d - T_w)}{p_{s,T_d}} \qquad \text{(A.5)}$$

where

p_{s,T_w} = the saturation vapor pressure at the wet bulb temperature (in hPa; see Eq. A.8)

$A =$ the psychrometer coefficient = 0.00066(1+0.00115 T_w) (in K^{-1})

$T_d =$ the dry bulb temperature (in Celsius degrees)

$T_w =$ the wet bulb temperature (in Celsius degrees)

$p_{s,T_d} =$ the saturation vapor pressure at the dry bulb temperature (in hPa; see Eq. A.9).

In Equation (A5) the saturation vapor pressures of pure water vapor over a plane surface of water at the web-bulb temperature T_w and the dry-bulb temperature T_d are calculated as follows [4]:

$$p_{s,Tw}\,[\text{or } p_{s,Td}] = \exp\left[\sum_{i=0}^{6} g_i \left(273.15 + T_w \;[\text{or } T_d]\right)^{i-2} + g_7 \ln\left(273.15 + T_w \;[\text{or } T_d]\right)\right] \qquad \text{(A.6)}$$

where the coefficients of six terms for the polynomial portion and the additional term before the natural logarithm are shown in the following table.

[3] ASTM (2015). *Standard Test Method for Measuring Humidity with a Psychrometer (the Measurement of Wet- and Dry-Bulb Temperatures)*, E337-15, ASTM International, West Conshohocken, PA.

[4] Wexler, A. (1976). "Vapor Pressure Formulation for Water in Range 0 to 100 °C." *Journal of Research of the National Bureau of Standards-A. Physics and Chemistry*, 80A(5 and 6), 775-785.

This publication is available free of charge from: https://doi.org/10.6028/NIST.TN.1994

This publication is available free of charge from: https://doi.org/10.6028/NIST.TN.1994

Table.A.2. Values for the coefficients in Eq. A.6.

Coefficient	Value
g_0	-0.29912729×10^4
g_1	-0.60170128×10^4
g_2	0.1887643854×10^2
g_3	$-0.28354721 \times 10^{-1}$
g_4	$0.17838301 \times 10^{-4}$
g_5	$-0.84150417 \times 10^{-9}$
g_6	$0.44412543 \times 10^{-12}$
g_7	0.2858487×10^1

For considering effects of ambient pressure deviation from the standard atmospheric pressure (101325 Pa) on the relative humidity, the correction based on ASTM E337-15[5] is used to Eq. (A.5):

$$RH = RH_o + B(T_d - T_w)(101325 - p) \quad \text{(A.7)}$$

where

$B =$ the correction factor for relative humidity due to atmospheric pressure deviation

$p =$ the measured atmospheric pressure [Pa]

This correction allows for deviations from atmospheric pressure up to approximately 30%. This method is applicable from 5 ˚C to 50 ˚C, still within the experimental bounds. The values for the

[5] ASTM (2015). *Standard Test Method for Measuring Humidity with a Psychrometer (the Measurement of Wet- and Dry-Bulb Temperatures)*, E337-15, ASTM International, West Conshohocken, PA.

This publication is available free of charge from: https://doi.org/10.6028/NIST.TN.1994

correction factor, *B*, at a measured dry bulb temperature can be calculated by using interpolation from Table X4.1 in the ASTM standard (see Figure A.1):

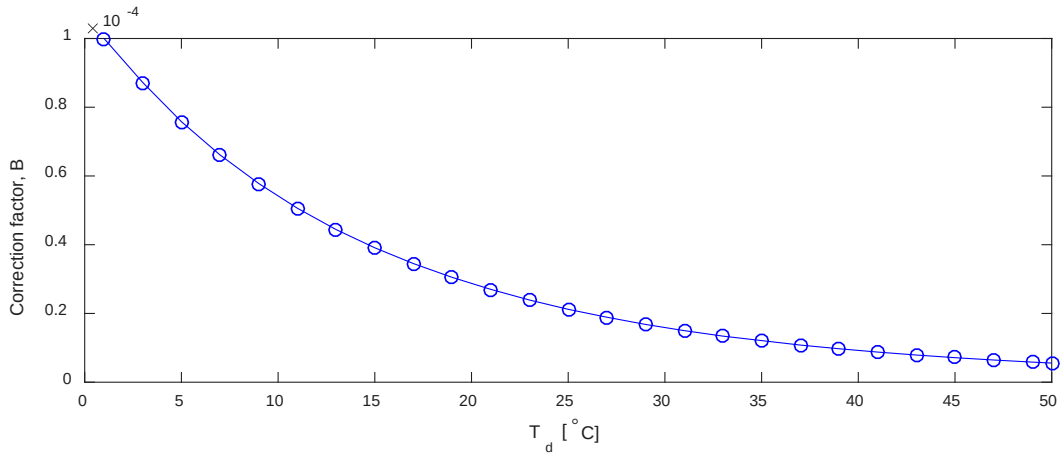

Figure A.1. Correction factor (*B*) from Table X4.1 in ASTM E337-15.

An example calculation is presented in two cases to illustrate the calculation of the relative humidity of air under atmospheric pressure above and below 101325 Pa.

Example 1.

Assuming that the ambient temperature is T_d = 20 ˚C, the ambient atmospheric pressure P = 90000 Pa and the wet bulb temperature T_w = 18.9˚C, the relative humidity of the air can be calculated (Eq. A.7):

$$\mathrm{RH} = \frac{p_{s,Tw} - A P_{st}\left(T_d - T_w\right)}{p_{s,Td}} + \frac{B\left(T_d - T_w\right)\left(p_{st} - p\right)}{100}$$

$$= 0.9053$$

where

The saturation pressure of water vapor at the wet-bulb temperature T_w is (Eq. A.6)

$$p_{s,Tw} = \exp\left[\sum_{i=0}^{6} g_i \left(273.15 + T_w\right)^{i-2} + g_7 \ln\left(273.15 + T_w\right)\right] = 2183.9\,[\mathrm{Pa}]$$

The psychrometric coefficient is:

$$A = 6.60 \times 10^{-4}\left(1 + 0.00115 T_w\right) = 0.000668$$

The saturation pressure of water vapor at the ambient temperature T_d is (Eq. A.10):

$$p_{s,Td} = \exp\left[\sum_{i=0}^{6} g_i \left(273.15 + T_d\right)^{i-2} + g_7 \ln\left(273.15 + T_d\right)\right] = 2338.5\,[\text{Pa}]$$

The correction factor B at T_d = 20 ˚C (Figure A.1) is:

$B = 2.8695 \times 10^{-5}$

The standard atmospheric pressure is:

p_{st} = 101325 [Pa].

Note: The relative humidity in the program using REFPROP is 0.905356.

Example 2.

Assuming that the ambient temperature is T_d = 31 ˚C, the ambient atmospheric pressure is P = 131722 Pa and the wet bulb temperature is T_w = 16.9˚C, the relative humidity of the air can be calculated below (Eq. A.7):

$$\text{RH} = \frac{p_{s,Tw} - A P_{st}\left(T_d - T_w\right)}{p_{s,Td}} + \frac{B\left(T_d - T_w\right)\left(p_{st} - p\right)}{100}$$
$$= 0.1502$$

where

The saturation pressure of water vapor at the wet-bulb temperature T_w is (Eq. A.6)

$$p_{s,Tw} = \exp\left[\sum_{i=0}^{6} g_i \left(273.15 + T_w\right)^{i-2} + g_7 \ln\left(273.15 + T_w\right)\right] = 1925.5\,[\text{Pa}]$$

The psychrometric coefficient is:

$$A = 6.60 \times 10^{-4}\left(1 + 0.00115 T_w\right) = 0.000673$$

The saturation pressure of water vapor at the ambient temperature T_d (Eq. A.6) is:

$$p_{s,Td} = \exp\left[\sum_{i=0}^{6} g_i \left(273.15 + T_d\right)^{i-2} + g_7 \ln\left(273.15 + T_d\right)\right] = 4495.0\,[\text{Pa}]$$

The correction factor B at T_d = 31 ˚C (Figure A.1) is:

$B = 1.5000 \times 10^{-5}$

This publication is available free of charge from: https://doi.org/10.6028/NIST.TN.1994

The standard atmospheric pressure is:

p_{st} = 101325 [Pa].

Note: The relative humidity in the program using REFPROP is 0.150369.

The results in the two examples show that both the REFPROP and the ASTM standard methods can calculate the relative humidity of air to within differences of less than about 0.001%.

This publication is available free of charge from: https://doi.org/10.6028/NIST.TN.1994

This publication is available free of charge from: https://doi.org/10.6028/NIST.TN.1994

APPENDIX B.
LUMPED-ELEMENT TRANSMISSION LINE MODEL FOR ACOUSTIC PROPAGATION IN TUBES

The theory of acoustic waves in gas-filled tubes was first proposed by Kirchhoff [1] and describes the coupling between acoustic, thermal, and vorticity waves. Kirchhoff's original paper included the solution for the specific case of a tube with circular cross section. A modern formulation of Kirchhoff's theory in the low-frequency limit, generally attributed to Crandall [2], is analogous to the theory of plane wave propagation in lossy electromagnetic transmission lines. The solution outlined here is a lumped-element model for a finite-length transmission line that uses a T-network [3] to represent the distributed impedances so that the acoustic pressure p and acoustic volume velocity U can be determined using standard circuit analysis; the model is valid for acoustic wave propagation in a system of circular tubes below the cutoff frequency for transverse modes, i.e., $ka_j < 1.84$, where k is the wavenumber ($k = \omega/c$), and a_j is the largest tube radius. We implicitly assume $e^{i\omega t}$ time dependence ($i = \sqrt{-1}$). Here we neglect end effects due to the radiation impedance and non-planar waves at the ends of tube sections that result in small effective-length corrections and additional energy loss. End effects can be included by the addition of a series impedance Z_{end} at each junction. (See Gillis et al.[4], for example.)

Lossy propagation of acoustic waves in a gas-filled cylindrical tube with cross-sectional area A have a characteristic impedance Z_0 and propagate in the ± z (axial) direction with a z-dependence proportional to $e^{\pm\Gamma z}$ where Γ is the propagation parameter. Z_0 and Γ are given by

---

[1] Kirchhoff, G. (1868). "Über den Einfluss der Wärmeleitung in einem Gase auf die Schallbewegung," *Ann. Phys. Chem.* 134, 177; English translation ''On the influence of heat conduction in a gas on sound propagation,'' in *Benchmark Papers in Acoustics: Physical Acoustics*, edited by R. B. Lindsay (Dowden, Hutchinson, & Ross, Stroudsburg, Pennsylvania, 1974), p. 7.

[2] Crandall, I. B. (1927). *Theory of Vibrating Systems and Sound*. Van Nostrand, New York, pp. 229–241.

[3] Mawardi, O.K. (1949) "On the propagation of sound waves in narrow conduits," *J. Acoust. Soc. Am.* **21**, 482–486.

[4] Gillis, K.A., Mehl, J.B., and Moldover, M.R. (2003). "Theory of the Greenspan viscometer," *J. Acoust. Soc. Am.* **114**, 166–173

$$Z_0 = \frac{\rho c}{A}\frac{1}{\sqrt{\left[1+(\gamma-1)F_t\right](1-F_v)}}, \qquad \Gamma = ik\sqrt{\frac{1+(\gamma-1)F_t}{1-F_v}} \ . \tag{B.1}$$

In Eq. (B.1), the gas properties are the mass density ρ, the speed of sound c, and the heat capacity ratio $\gamma = C_P/C_V$. The attenuation of the acoustic waves occurs near the tube wall due to thermal conduction and viscous shear. Energy loss due to thermal conduction is included in the circular loss function F_t given by

$$F_t = \frac{2J_1(\kappa_t a)}{\kappa_t a J_0(\kappa_t a)}, \qquad \kappa_t = (1-i)/\delta_t \tag{B.2}$$

where J_m is the m^{th} order Bessel function, $\delta_t = \sqrt{2D_t/\omega}$ is the thermal penetration length, D_t is the thermal diffusivity, and a is the tube radius. Energy loss due to viscosity is included in the function F_v which is identical to Eq. (B.2) but with δ_t replaced by the viscous penetration length $\delta_v = \sqrt{2D_v/\omega}$, where D_v is the viscous diffusivity (kinematic viscosity).

The equivalent circuit for acoustic waves in a tube with length L, radius a, and terminated with an impedance Z_L is shown in Fig. A1. Sound enters the tube at the left end ($z = 0$) where the acoustic

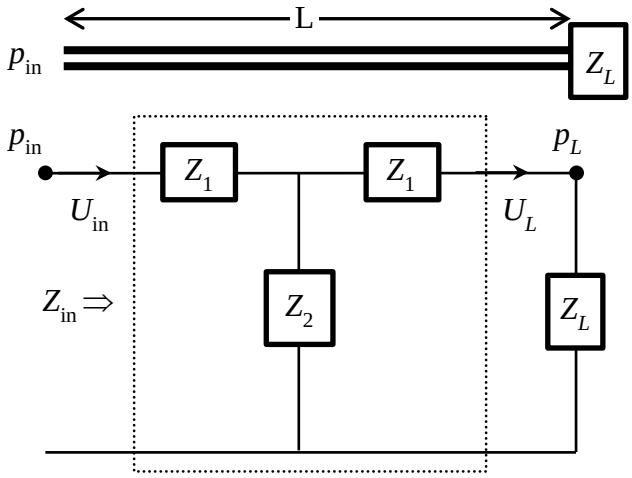

Figure B.1 T-network equivalent circuit for acoustic wave propagation in a finite-length cylindrical tube.

input impedance that the wave "sees" is Z_{in}; the wave propagates down the length of the tube, where (at $z = L$) the tube is terminated by the acoustic load impedance Z_L; a portion of the wave reflects back and the rest is transmitted or dissipated. The load impedance could be, for example,

This publication is available free of charge from: https://doi.org/10.6028/NIST.TN.1994

another section of tubing, a chamber, or a transducer. The impedances Z_1 and Z_2 in the T-network are functions of Z_0 and Γ, namely

$$Z_1 = Z_0 \tanh\left(\tfrac{1}{2}\Gamma L\right), \quad Z_2 = \frac{Z_0}{\sinh(\Gamma L)} \ . \tag{B.3}$$

Analysis of the circuit in Fig. B.1 and Eq. (B.3) gives, after some manipulation, the important results for the input impedance

$$Z_{\text{in}} = Z_0 \frac{Z_{\text{L}} + Z_0 \tanh(\Gamma L)}{Z_0 + Z_{\text{L}} \tanh(\Gamma L)} \ , \tag{B.4}$$

the volume velocities

$$U_{\text{in}} = \frac{p_{\text{in}}}{Z_{\text{in}}}, \qquad U_{\text{L}} = \frac{p_{\text{L}}}{Z_{\text{L}}} \ , \tag{B.5}$$

and the transfer function

$$\frac{p_{\text{in}}}{p_{\text{L}}} = \frac{Z_{\text{in}}}{Z_{\text{L}}}\left[1 + \frac{Z_{\text{L}}}{Z_0}\tanh(\Gamma L)\right]\cosh(\Gamma L) = \left[1 + \frac{Z_0}{Z_{\text{L}}}\tanh(\Gamma L)\right]\cosh(\Gamma L) \ . \tag{B.6}$$

These results can be cast into matrix form

$$\begin{pmatrix} U_{\text{in}} \\ p_{\text{in}} \end{pmatrix} = \begin{pmatrix} \cosh(\Gamma L) & \dfrac{1}{Z_0}\sinh(\Gamma L) \\ Z_0 \sinh(\Gamma L) & \cosh(\Gamma L) \end{pmatrix} \begin{pmatrix} U_{\text{L}} \\ p_{\text{L}} \end{pmatrix} \tag{B.7}$$

which, together with the boundary conditions in Eq. (B.5), contains the results in Eqs. (B.4) and (B.6). The matrix formulation simplifies the analysis of systems with multiple sections of tubing with different lengths or radii. In general, each section will have its own propagation constant and characteristic impedance because the loss functions are dependent on the tube radius. However, the gas properties, the frequency ω, and the wavenumber k are necessarily the same throughout the system.

This publication is available free of charge from: https://doi.org/10.6028/NIST.TN.1994

This publication is available free of charge from: https://doi.org/10.6028/NIST.TN.1994

The model for the multiple tube system represented in Fig. 2.2 has the equivalent circuit for the j^{th} and $(j+1)^{th}$ sections shown in Fig. B.2. The j^{th} section has a tube (length L_j, diameter $2a_j$) and a transducer volume (V_{Tj}). Because the length of the transducer volume is considered to be much smaller than the wavelength of sound, the acoustic inertance and the viscous loss described by the series impedance Z_1 for the transducer volume is negligible compared to the acoustic compliance and the thermal loss described by the parallel impedance Z_2. Thus, the transducer impedance $Z_{T,j}$ appears as a parallel impedance in Fig. B.2.

The transfer function p_{j-1}/p_j from Fig. B.2 is

$$\frac{p_{j-1}}{p_j} = \cosh\left(\Gamma_j L_j\right) + \sinh\left(\Gamma_j L_j\right)\frac{Z_{0,j}}{Z_{T,j}} + \frac{\sinh\left(\Gamma_j L_j\right)}{\sinh\left(\Gamma_{j+1} L_{j+1}\right)}\frac{Z_{0,j}}{Z_{0,j+1}}\left[\cosh\left(\Gamma_{j+1} L_{j+1}\right) - \frac{p_{j+1}}{p_j}\right] \quad \text{(B.8)}$$

which follows from the node equation for volume velocity $U_{T,j} = U'_j - U_{j+1}$, the input impedance to section j+1, $Z_{\text{in},j+1}$

$$Z_{\text{in},j+1} = Z_{0,j+1}\frac{1+\left(Z_{0,j+1}/Z_{L,j+1}\right)\tanh\left(\Gamma_{j+1} L_{j+1}\right)}{\left(Z_{0,j+1}/Z_{L,j+1}\right)+\tanh\left(\Gamma_{j+1} L_{j+1}\right)}\ , \quad \text{(B.9)}$$

and the transfer function for section j+1 [Eq. (B.6)] to eliminate $Z_{\text{L},j+1}$. For a system with N sections, the complete transfer function is

$$\frac{p_{\text{in}}}{p_N} = \frac{p_{\text{in}}}{p_1}\frac{p_1}{p_2}\cdots\frac{p_{N-1}}{p_N} = \left[\prod_{j=1}^{N-1}\frac{p_{j-1}}{p_j}\right]\times\frac{p_{N-1}}{p_N} \quad \text{(B.10)}$$

with p_{j-1}/p_j given by Eq. (B.8) for $j \neq N$ and

$$\frac{p_{N-1}}{p_N} = \cosh\left(\Gamma_N L_N\right) + \sinh\left(\Gamma_N L_N\right)\frac{Z_{0,N}}{Z_{T,N}}. \quad \text{(B.11)}$$

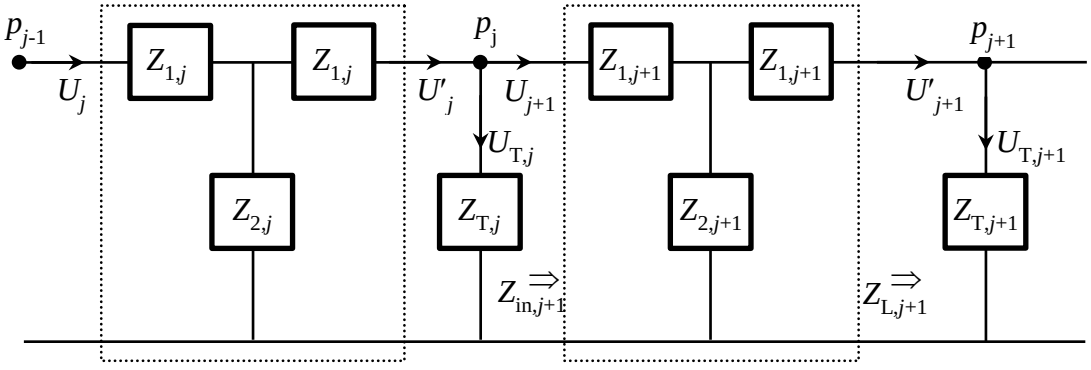

Fig. B.2 Equivalent circuit for sections j and j+1 of the system in Fig. 2.2.

Equation (B.8) is equivalent to Eq. 2.1 with the identifications

$$\vartheta_j \to \Gamma_j \tag{B.12a}$$

$$n_j \to \frac{\gamma}{1+(\gamma-1)F_{t,j}} \tag{B.12b}$$

$$\alpha_j \to (1-i)a_j/\delta_v \tag{B.12c}$$

$$\frac{J_0(\alpha_j)}{J_2(\alpha_j)} \to -\frac{1}{1-F_{v,j}} \tag{B.12d}$$

$$\frac{V_{t,j+1}\vartheta_{j+1}L_j J_0(\alpha_j)J_2(\alpha_{j+1})}{V_{t,j}\vartheta_j L_{j+1}J_2(\alpha_j)J_0(\alpha_{j+1})} \to \frac{Z_{0,j}}{Z_{0,j+1}} \tag{B.12e}$$

Transducer impedance

In many instances we can model a transducer's impedance as a compliant volume V_T of gas with surface area S_T. At frequencies below any resonances of the transducer volume, but δ_t is still much smaller than any dimension of the transducer volume, the impedance is approximately [5]

$$Z_T \approx \frac{\rho c^2}{i\omega V_T}\frac{1}{\left[1+(1-i)(\gamma-1)S_T\delta_t/(2V_T)\right]} \ . \tag{B.13}$$

Equation (B.13) must be modified if δ_t is comparable to a dimension ℓ of the volume. In the low frequency limit, the gas expansion/compression is isothermal instead of adiabatic, therefore the quantity in the square bracket in Eq. (B.13) should approach γ as δ_t increases above about 0.1ℓ, but it does not. The general relationship between the pressure change δp and the density change $\delta\rho$ is sometimes described in terms of a "polytropic parameter" k_p such that $\delta p = \delta\rho\, c^2 k_p/\gamma$ where k_p varies from 1 for isothermal expansion to γ for adiabatic expansion. (See Fig. B.3.) Thus, the modified impedance for a transducer volume becomes

$$Z_T = \frac{\rho c^2}{i\omega V_T}\frac{k_p}{\gamma} = \frac{\rho c^2}{i\omega V_T}\frac{1}{\left[1+(\gamma-1)F_{t,T}\right]} \ , \tag{B.14}$$

[5] F.B. Daniels, "Acoustical impedance of enclosures," J. Acoust. Soc. Am. **19**, 569-570 (1947).

This publication is available free of charge from: https://doi.org/10.6028/NIST.TN.1994

This publication is available free of charge from: https://doi.org/10.6028/NIST.TN.1994

where k_p is a complex-valued, frequency-dependent polytropic parameter and $F_{t,\mathrm{T}}$ is thermal loss function for the transducer volume. Since the wavelength of sound is significantly longer than any dimension of the volume, we anticipate that $F_{t,\mathrm{T}}$ is not strongly geometry dependent.

For a spherical volume with radius b, the calculated low-frequency impedance [6] is

$$Z_{\mathrm{T,sphere}} = \frac{\rho c^2}{i\omega V_{\mathrm{T}}} \frac{1}{\left[1+(\gamma-1)F_{t,\mathrm{sphere}}\right]}\ , \tag{B.15a}$$

where $$F_{t,\mathrm{sphere}} = \frac{3}{\beta^2 b^2}\left[\beta b \coth(\beta b) - 1\right], \qquad \beta \equiv (1+i)/\delta_t\ . \tag{B.15b}$$

$Z_{\mathrm{T,sphere}}$ form Eq. (B.15a) has the correct limiting behavior for $\delta_t \to 0$, i.e. $F_{t,\mathrm{sphere}} \approx (1-i)S\delta_t/(2V) \to 0$ and the correct limiting behavior as δ_t approaches and exceeds b ($F_{t,\mathrm{sphere}} \to 1$). Thus, the polytropic parameter for a spherical volume is

$$k_p = \frac{\gamma}{1+(\gamma-1)F_{t,\mathrm{sphere}}} \to \begin{cases} \gamma \text{ for } F_{t,\mathrm{sphere}} \to 0 \text{ (adiabatic)} \\ 1 \text{ for } F_{t,\mathrm{sphere}} \to 1 \text{ (isothermal)} \end{cases}\ . \tag{B.16}$$

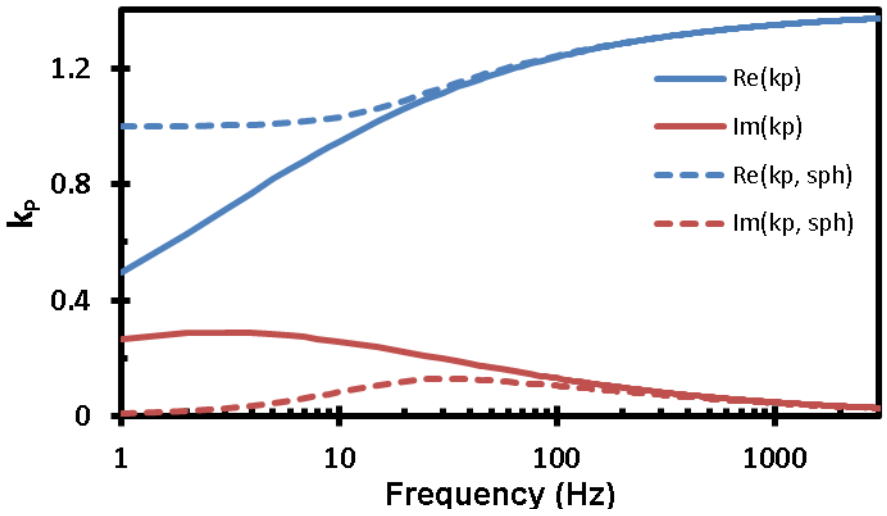

Figure B.3 (solid curves) The "effective" polytropic constant used in the approximation in Eq. (B.13). This approximation predicts the correct high-frequency (adiabatic) limit ($k_p \to \gamma$), but it does not predict the correct low-frequency (isothermal) limit. (dashed curves) The polytropic constant for a spherical geometry (Eqs. B.15a - 16) has the correct low-and high-frequency limits.

[6] F.B. Daniels, "Acoustical impedance of enclosures," J. Acoust. Soc. Am. **19**, 569 (1947).

This publication is available free of charge from: https://doi.org/10.6028/NIST.TN.1994

The effect on the calculated dynamic pressure ratio of various approximations to the polytropic constant is shown in Fig. B.4.

Cylindrical volumes are problematic when estimating the low-frequency impedance from a summation of side and endplate admittances. At the corners, the side and endplate boundary layers overlap resulting in an overestimate of the boundary layer's effect. When δ_t is small compared to the dimensions, this overestimate is negligible and Eq. (B.13) is obtained; however when δ_t is large, this summation gives the wrong isothermal limit. Fortunately, the surface area-to-volume ratio for a cylindrical volume whose length L equals its diameter $2a$ is $S/V = 3/a$, which is the same ratio as a sphere with the same radius, $b = a$. Thus, the impedance of a right, equilateral cylindrical volume with radius a has the same limiting behavior, to $O(\delta_t/a)$ at high frequency and to $O(a/\delta_t)$ at low frequency, as a spherical enclosure with the same radius. Furthermore, we propose that the

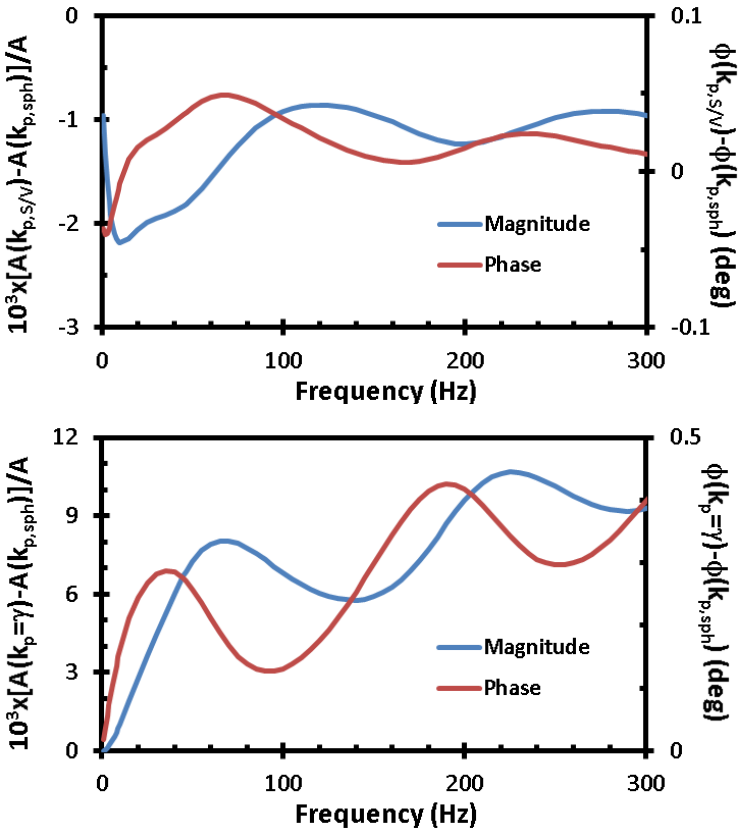

Figure B.4 (Top) The calculated dynamic pressure ratio $|P_T/P_0|$ changes by 0.1 % to 0.2 % when the approximation [Eq. (B.14)] for the polytropic constant is used instead of the exact form for a spherical volume [Eq. (B.16)]. (Bottom) When the polytropic constant is approximated as a constant ($k_p = \gamma$), the calculated dynamic pressure changes by about 1 %.

differences between the impedances at intermediate frequencies are small enough to be ignored. Therefore, we approximate the impedance of a cylindrical transducer volume (that is nearly equilateral) using Eq. (B.15a) for a sphere with the same S/V, i.e. $b = 3V/S$ and $F_{t,\mathrm{T}} \approx F_{t,\mathrm{sphere}}$. With this approximation, the impedance will have the correct limiting behavior in the adiabatic and isothermal limits.

Because impedances can get very large, it is sometimes desirable to work with dimensionless admittances (reciprocal of impedance) for numerical computation. We define a specific characteristic admittance for tube j with cross sectional area $A_j = \pi\, a_j^2$

$$y_{0,j} \equiv \frac{\rho c}{A_j Z_{0,j}} = \sqrt{\left[1+(\gamma-1)F_{t,j}\right]\left(1-F_{v,j}\right)} \tag{B.17}$$

In Eqs. (B.8) and (B.9), each section of tube has a different diameter, so the specific admittances must be scaled by the appropriate areas. In terms of specific admittances, Eqs. (B.8) and (B.11) become

$$\frac{p_{j-1}}{p_j} = \cosh\left(\Gamma_j L_j\right) + \sinh\left(\Gamma_j L_j\right)\frac{y_{T,j}}{y_{0,j}} + \frac{\sinh\left(\Gamma_j L_j\right)}{\sinh\left(\Gamma_{j+1} L_{j+1}\right)}\frac{A_{j+1}}{A_j}\frac{y_{0,j+1}}{y_{0,j}}\left[\cosh\left(\Gamma_{j+1} L_{j+1}\right) - \frac{p_{j+1}}{p_j}\right] \tag{B.18}$$

$$\frac{p_{N-1}}{p_N} = \cosh\left(\Gamma_N L_N\right) + \sinh\left(\Gamma_N L_N\right)\frac{y_{T,N}}{y_{0,N}} \tag{B.19}$$

$$y_{\mathrm{T},j} \equiv \frac{\rho c}{A_j Z_{\mathrm{T},j}} = ikL_j\frac{V_{\mathrm{T},j}}{V_j}\left[1+(\gamma-1)F_{t,\mathrm{sphere}}\right] \tag{B.20}$$

where we define the volume of the j^{th} tube as $V_j = A_j L_j$ with area A_j and length L_j.

Tube resonances

Resonances in the tubes are usually undesirable. If the system of tubes is used in a probe microphone with the load impedance Z_{L} due to a transducer, then the response function must be corrected for the presence of resonances in the tube in order to obtain an accurate measurement of p_{in}. Resonances occur when $p_{\mathrm{in}}/p_{\mathrm{L}} = 0$ (or $p_{\mathrm{L}}/p_{\mathrm{in}} \to \infty$) in complex-frequency space. The zeros of Eq. (B.6) or (B.10) are a set of complex frequencies $\hat{f}_n = f_n + ig_n$ for which f_n is the resonance frequency and g_n is the half-width.

This publication is available free of charge from: https://doi.org/10.6028/NIST.TN.1994

For a simple system with just one tube and one volume, the transfer function Eq. (B.10) simplifies to

$$\frac{p_{\text{in}}}{p_{\text{L}}} = \left[1 + \frac{y_{\text{T}}}{y_0}\tanh(\Gamma L)\right]\cosh(\Gamma L) \tag{B.21}$$

and the condition for resonance becomes

$$1 + \frac{y_{\text{T}}}{y_0}\tanh(\Gamma L) = 0 \tag{B.22}$$

or, after substituting from Eqs. (B.1), (B.17), and (B.20), we have

$$\hat{k}L\tan\left(\hat{k}L\sqrt{\frac{1+(\gamma-1)F_t}{1-F_v}}\right) = \frac{V_{\text{tube}}}{V_{\text{T}}}\frac{\sqrt{\left[1+(\gamma-1)F_t\right](1-F_v)}}{1+(\gamma-1)F_{t,\text{sphere}}} \ . \tag{B.23}$$

In Eq. (B.23), $\hat{k}$ represents the complex-valued wavenumber that solves Eq. (B.22). For a Helmholtz mode to exist, $\hat{k}_{\text{H}}L << 1$ and therefore $V_{\text{tube}} << V_{\text{T}}$. In this case we can expand the tangent, keeping the first-order term, and solve for *k*

$$\hat{k}_{\text{H}} \approx \sqrt{\frac{A}{V_{\text{T}}L}\frac{1-F_v}{1+(\gamma-1)F_{t,\text{sphere}}}} \tag{B.24}$$

Additionally, if δ_v and δ_t are small, then (using $2\pi\hat{f} = \hat{k}c$)

$$\hat{f}_{\text{H}} = f_{\text{H}} + ig_{\text{H}} \approx \frac{c}{2\pi}\sqrt{\frac{A}{V_{\text{T}}L}}\left[1-(1-i)\frac{\delta_v}{2a}-(1-i)(\gamma-1)\frac{S_{\text{T}}\delta_t}{4V_{\text{T}}}\right] \tag{B.25}$$

Therefore,

$$f_{\text{H}} \approx \frac{c}{2\pi}\sqrt{\frac{A}{V_{\text{T}}L}}\left[1-\frac{\delta_v}{2a}-(\gamma-1)\frac{S_{\text{T}}\delta_t}{4V_{\text{T}}}\right], \qquad g_{\text{H}} \approx \frac{c}{2\pi}\sqrt{\frac{A}{V_{\text{T}}L}}\left[\frac{\delta_v}{2a}+(\gamma-1)\frac{S_{\text{T}}\delta_t}{4V_{\text{T}}}\right] \tag{B.26}$$

to lowest order in δ_v and δ_t. If $V_{tube} << V_T$, then the Helmholtz mode described above will be the lowest frequency mode. On the other hand, if $V_{tube} >> V_T$, then the lowest frequency mode will likely be a mode of the tube.

According to Eq. (B.23), if $V_{tube}/V_T >> 1$, we expect the solution for *kL* to be just below $\pi/2$.

Let

$$\sqrt{\frac{1+(\gamma-1)F_t}{1-F_v}} = 1+\Delta \tag{B.27}$$

This publication is available free of charge from: https://doi.org/10.6028/NIST.TN.1994

$$\hat{k}L\tan\left[\hat{k}L(1+\Delta)\right]=\frac{V_{tube}}{V_T}\frac{\sqrt{\left[1+(\gamma-1)F_t\right](1-F_v)}}{1+(1-i)(\gamma-1)S_T\delta_t/(2V_T)} \tag{B.28}$$

Assume $|\Delta|<<1$

$$\hat{k}L=\frac{\pi}{2}(1-\varepsilon)\approx\frac{\pi}{2}\left(1-\frac{V_T}{V_{tube}}-(1-i)(\gamma-1)\frac{\delta_t}{2a}-(1-i)\frac{\delta_v}{2a}\right) \tag{B.29}$$

In this limit, we see that the lowest resonance is a quarter-wave mode of the tube with

$$f_r\approx\frac{c}{4L}\left[1-\frac{V_{\mathrm{T}}}{V_{\mathrm{tube}}}-(\gamma-1)\frac{\delta_t}{2a}-\frac{\delta_v}{2a}\right],\qquad g_r\approx\frac{c}{4L}\left[(\gamma-1)\frac{\delta_t}{2a}+\frac{\delta_v}{2a}\right] \tag{B.30}$$

In the lumped element model, this limit is equivalent to $Z_{\mathrm{T}}>>Z_0$ (or $y_{\mathrm{T}}<<y_0$).

$$\frac{Z_{\mathrm{T}}}{Z_0}=\frac{y_0}{y_{\mathrm{T}}}\approx\frac{1}{ikL}\frac{V_{\mathrm{tube}}}{V_{\mathrm{T}}} \tag{B.31}$$

Near the lowest mode, $kL\sim1$, the tube is terminated by a high impedance thereby forming a quarter-wave resonator in the tube. At sufficiently high frequency $kL>>V_{\mathrm{tube}}/V_{\mathrm{T}}$, the impedance ratio goes to zero and the tube becomes a half-wave resonator.

Finally, sound waves propagating down a long tube are damped out over a characteristic distance called the attenuation length l_a. The attenuation length is the distance over which the pressure amplitude is attenuated to 1/e of its initial value. For a wave traveling in the +z-direction in a long tube, the acoustic pressure is $p\propto\exp\left\{-\left[\mathrm{Re}(\Gamma)+i\,\mathrm{Im}(\Gamma)\right]z\right\}$, so the attenuation length is

$$l_a=\frac{1}{\mathrm{Re}(\Gamma)}\ . \tag{B.32}$$

A wave that is propagating in a tube that is significantly longer than l_a will be damped out before it reaches the end of the tube. Note that l_a is frequency dependent: it gets shorter as the frequency is increased, i.e., the wave is damped over a shorter distance.

This publication is available free of charge from: https://doi.org/10.6028/NIST.TN.1994